Chemical Geology 502 (2018) 107–121

Contents lists available at ScienceDirect

Chemical Geology

journal homepage: www.elsevier.com/locate/chemgeo

The 825 Ma Yiyang high–MgO basalts of central South China: Insights from Os–Hf–Nd data

Tao Wu[a,c], Xuan-Ce Wang[b,c,*], Wu-Xian Li[d], Simon A. Wilde[b], Liyan Tian[e,f], Chong-Jin Pang[g], Jie Li[d]

[a] Ocean College, Zhejiang University, 1 Zheda Road, Zhoushan 316021, China
[b] The School of Earth Science and Resources, Chang'an University, Xi'an 710054, China
[c] The Institute for Geoscience Research, Department of Applied Geology, Curtin University, GPO Box U1987, Perth, WA 6845, Australia
[d] State Key Laboratory of Isotope Geochemistry, Guangzhou Institute of Geochemistry, Chinese Academy of Sciences, Guangzhou 510640, China
[e] Institute of Deep-Sea Science and Engineering, Chinese Academy of Sciences, Sanya 572000, China
[f] Laboratory for Marine Geology, Qingdao National Laboratory for Marine Science and Technology, Qingdao 266061, China
[g] Collaborative Innovation Center for Exploration of Hidden Nonferrous Metal Deposits and Development of New Materials in Guangxi, College of Earth Sciences, Guilin University of Technology, Guilin 541004, China

ARTICLE INFO

Editor: Catherine C.

Keywords:
Neoproterozoic
Komatiitic basalts
Plume–derived magma
Recycled sediments
South China Block
Rodinia

ABSTRACT

High–MgO basaltic lavas, including komatiites and picrites, have long been used as probes of both the chemical and thermal evolution of the mantle through time. The ca. 825 Ma Yiyang high–MgO basalts in the central South China Block (SCB) were considered to be the first evidence for > 1500 °C mantle melts by a Rodinian mantle plume. However, later studies proposed that they may have been generated within an arc setting and can be classified as boninites. Here we present a comprehensive Os–Hf–Nd isotopic study of the Yiyang basalts. The Yiyang basalts have high MgO (> 10%), Ni (> 182 ppm), Cr (> 667 ppm) and Os contents (mostly > 0.3 ppb) with radiogenic Os isotopes ($(^{187}Os/^{188}Os)_i$ = 0.134 to 0.282). They have relatively uniform whole–rock Nd and Hf isotopes with $\varepsilon_{Nd}(t)$ and $\varepsilon_{Hf}(t)$ values ranging from −3.7 to −1.3 and from +2.9 to +4.3, respectively. Our new data indicate that although crustal assimilation and fractional crystallization (AFC) may have played a role in the geochemical diversity of the Yiyang basalts, the enrichment in light rare earth elements (LREE) and large–ion lithophile elements (LILE) relative to high field strength elements (HSFE) most likely are features of the primary magma. The Yiyang high–MgO basalts, along with contemporary high–MgO basalts in the central SCB, have lower SiO_2 contents, and Al_2O_3/TiO_2 ratios, but higher TiO_2, Zr, Nb, and Nd contents and Th/U ratios than typical boninites. The presence of negative Ba anomalies and depletion in middle REE (MREE) to heavy REE (HREE) in these high-MgO basaltic rocks are also distinct from what is observed in typical boninites. Therefore, the primary magma of the Yiyang basalts had similar whole–rock geochemical compositions to that of komatiites and plume–derived basalts. Their decoupled Hf—Nd isotopes indicate that recycled oceanic sediments may have been incorporated into their source. They have primitive mantle–like Al_2O_3/TiO_2 ratios (21 − 23) and flat HREE patterns. However, unlike other Al–undepleted or Munro–type komatiites, their mantle source did not undergo earlier melting events. Our new results support the view that the Yiyang basalts are komatiitic and not boninitic, and that they were likely derived from a Rodinian mantle plume.

1. Introduction

High–MgO mafic lavas, including komatiite, komatiitic basalt, picrite, and boninite, can be generated in various tectonic settings. Although their petrogenesis is still open to debate (e.g. Herzberg, 1995; Arndt et al., 2008; Grove and Parman, 2004; Parman et al., 2004), they have long been used as probes of both the chemical and thermal evolution of the mantle through time (Grove and Parman, 2004; Wang et al., 2007; Sobolev et al., 2016).

The Re—Os isotope system is distinct from other radiogenic isotope systems in that the parent element (Re) is a moderately incompatible element that partitions readily from the mantle into magma during partial melting, whereas the daughter element (Os) is a highly compatible element that is retained in the residual mantle (Shirey and

* Corresponding author at: Department of Applied Geology, Curtin University, GPO Box U1987, Perth, WA 6845, Australia.
E-mail address: x.wang3@curtin.edu.au (X.-C. Wang).

https://doi.org/10.1016/j.chemgeo.2018.10.027
Received 24 January 2018; Received in revised form 28 October 2018; Accepted 30 October 2018
Available online 06 November 2018
0009-2541/

Walker, 1998). As a consequence, both oceanic and continental crusts have high Re/Os ratios, and have developed radiogenic Os isotope compositions over time. Therefore, the Re−Os isotope system is a particularly sensitive tracer of crustal components involved in basaltic magma petrogenesis (e.g. Widom, 2011; Suzuki et al., 2011).

The geochemical behavior of Lu−Hf parallels that of Sm−Nd in the mantle environment, leading to the correlation of $^{176}Hf/^{177}Hf$ with $^{143}Nd/^{144}Nd$ in most mantle (and crustal) rocks (e.g. Patchett et al., 1984; Blichert-Toft et al., 1999; Vervoort et al., 1999). Nevertheless, previous studies have shown that sediment–melt interaction during subduction changes the Sm/Nd ratios < 1%, but increases the Lu/Hf ratios about 47% relative to unmodified sediments (Stracke et al., 2003 and references therein). Consequently, recycled sediments would develop unradiogenic $^{143}Nd/^{144}Nd$ and relatively radiogenic $^{176}Hf/^{177}Hf$ ratios with time (e.g. Patchett et al., 1984; Vervoort et al., 1999; Chauvel et al., 2008). Thus, a comprehensive Os–Hf–Nd isotopic study of high–MgO mafic lavas has the potential to constrain the role of crustal contamination and enable an estimate to be made of the importance of recycled components in the mantle source and thereby to constrain the geodynamic environment.

As a part of the supercontinent Rodinia, the South China Block (SCB) contains extensive ca. 850–760 Ma magmatic rocks (e.g. Li et al., 2003a; Li et al., 2003b; Li et al., 2010a; Li et al., 2010b; Wang et al., 2009; Zhou et al., 2002; Zhao and Cawood, 2012). However, the petrogenesis and tectonic setting of these rocks still remain controversial. Both a mantle plume (Li et al., 2003a; Li et al., 2010a; Wang et al., 2007; Wang et al., 2008; Wang et al., 2009) and a subduction model (Zhou et al., 2002; Zhou et al., 2006) have been proposed to explain their genesis. Such competing interpretations have led to different explanations about the position of the SCB within Rodinia: either at the margin of Rodinia (Zhou et al., 2002; Cawood et al., 2013) or as a "missing link" between western Laurentia and Australia–East Antarctica (Li et al., 1995; Li et al., 2008 and references therein). Previous studies have documented several ca. 830 Ma high–MgO basaltic pillow lavas in the central SCB, including the ca. 825 Ma Yiyang komatiitic basalts and the ca. 840–830 Ma Sibao, Lushan, Zhangyuan and Shexian high–MgO basalts (Fig.1; Wang et al., 2007; Zhao and Zhou, 2013; Zhao and Asimow, 2014). These high–MgO basalts are very important for investigating the chemical and thermal evolution of the mantle beneath the Neoproterozoic SCB. However, their petrogenesis is also open to debate, as they have been considered to be either plume–derived komatiitic basalts (e.g. Wang et al., 2007; Wang et al., 2009) or arc–generated boninites (e.g. Zhao and Zhou, 2013; Zhao and Asimow, 2014).

Here we present new Os–Hf–Nd isotopic data for the Yiyang high–MgO basalts. Using existing geochemical data, we aim to investigate the effects of later geological processes (e.g. hydrothermal alteration, fractional crystallization and continental crustal contamination) on their whole–rock compositions, discuss how they differ from typical boninites, and constrain their petrogenesis and source.

2. Geological background and sample selection

The South China Block (SCB) was formed by amalgamation of the Yangtze and Cathaysia blocks during the ca. 1.1–0.9 Ga Sibao orogeny (e.g. Li et al., 1995; Li et al., 2007a; Li et al., 2009), although some researchers believe that this orogeny lasted until ca. 820 Ma or even later (e.g. Zhao and Cawood, 1999; Zhou et al., 2002; Zhao et al., 2011). This orogenic event is marked by an angular unconformity between the Lengjiaxi Group (or Sibao Group and its equivalents) and the overlying Banxi Group (or Danzhou Group and its equivalents) in the central South China Block (Wang and Li, 2003). The Lengjiaxi Group (~860–835 Ma) is composed of siltstone, graywacke, tuffaceous sandstone, with interbedded pyroclastics and lavas of flysch affinity (Wang et al., 2003; Zhang et al., 2015), whereas the Banxi Group (~810–720 Ma) comprises sandy conglomerate, arkose, carbonaceous slate and dolomite deposited in a littoral–neritic environment (Wang et al., 2003; Zhang et al., 2015), and is associated with bimodal volcanic rocks. The Banxi Group represents a typical mid–Neoproterozoic continental rift succession, developed within the Nanhua rift (NE–SW trending) between the Yangtze and Cathaysia blocks.

Large–scale magmatic events within and adjacent to these rift systems have been dated at ca. 830–740 Ma (Zhou et al., 2002, Zhou et al., 2006; Li et al., 2003a; Li et al., 2003b; Li et al., 2008; Wang et al., 2009), with two major phases of activity at ca. 825–800 and ca. 790–740 Ma (Li et al., 2003a; Wang et al., 2009). Amongst the first phase of magmatic rocks, the Yiyang high–MgO basalts from central South China have been interpreted as products of high–temperature

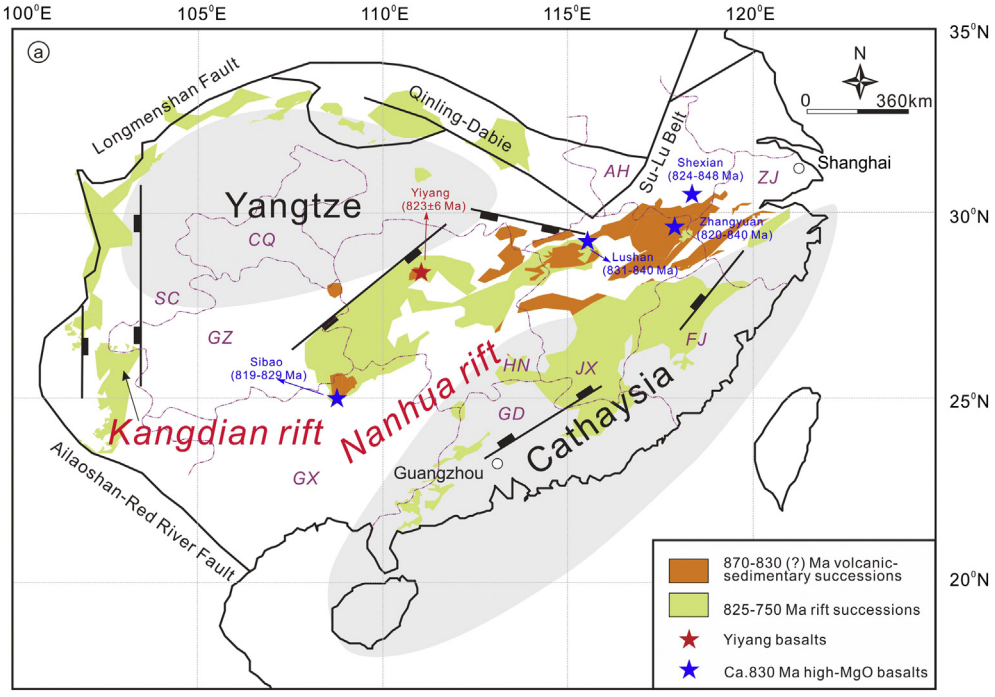

Fig. 1. Simplified map of South China showing the location of major tectonic units and the distribution of the ca. 830 Ma basaltic rock (modified after Wang and Li, 2003; Li et al., 2010b). ZJ–Zhejiang Province; AH–Anhui Province; JX–Jiangxi Province; HN–Hunan Province; GX–Guangxi Province; FJ–Fujiang Province; GD–Guangdong Province; CQ–Chongqing city; SC–Sichuan Province. Data sources: the ca. 830 Ma high–MgO basalts are from Zhao and Zhou (2013) and Zhao and Asimow (2014).

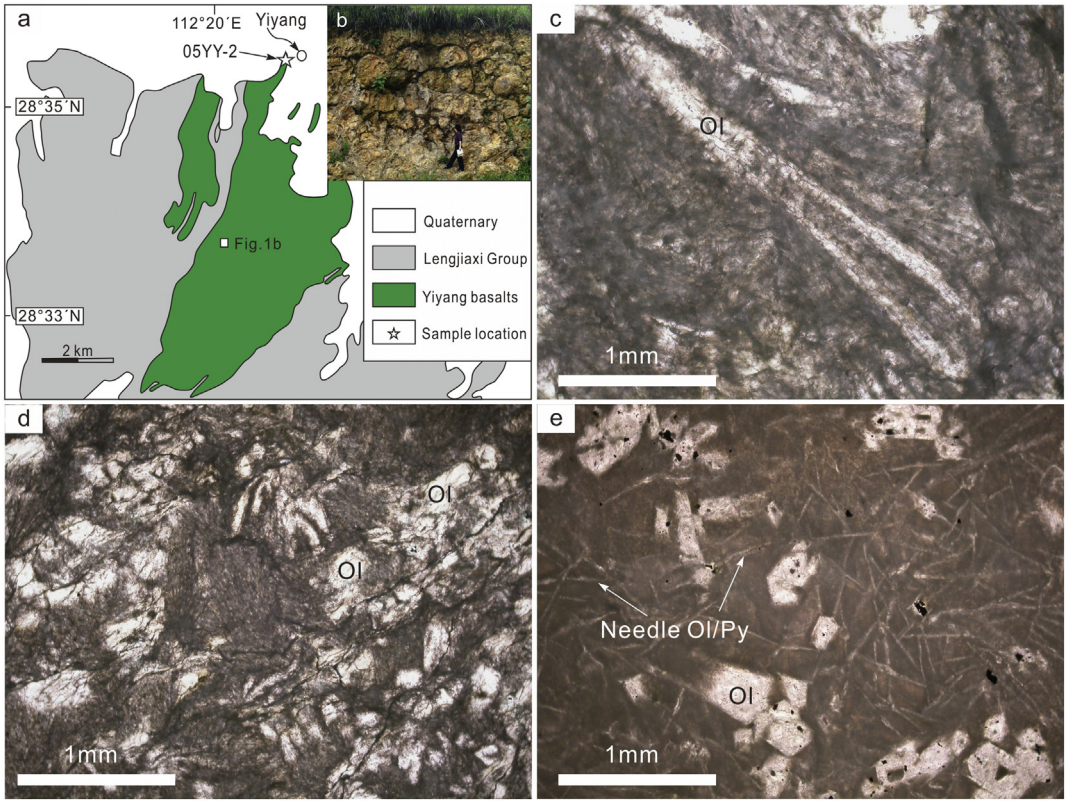

Fig. 2. (a) and (b) Simplified map showing the Yiyang basalts and sample location (after Wang et al., 2007). (c), (d) and (e) Photomicrographs show the skeletal olivine pseudomorphs with acicular olivine/clinopyroxene in the matrix of the Yiyang basalts. Ol–Olivine; Py–pyroxene. (b) and (c) are from Wang et al. (2007).

(> 1500 °C) melts related to a mantle plume (Wang et al., 2007) or else as arc–generated boninites (Zhao and Zhou, 2013; Zhao and Asimow, 2014). In recent years, more 850–860 Ma igneous rocks like alkaline complex (Li et al., 2010a), bimodal volcanic rocks (Li et al., 2010a; Lyu et al., 2017), granites (Wu et al., 2018) and etc. have been widely reported, indicating a major magmatic event at this time.

The Yiyang high–MgO basalts are well exposed around Yiyang city, with a total outcrop area of 17 km^2 (Fig. 2a). They are locally in fault contact with the Lengjiaxi Group, whereas their relationship with the Banxi Group is unclear (e.g. Guo et al., 2003; Che et al., 2005; Wang et al., 2007). SHRIMP U−Pb zircon dating of a highly evolved andesitic sample from the Yiyang high–MgO basalt suite gave an age of 823 ± 6 Ma, which is interpreted as the eruption age of these lavas (Wang et al., 2007). This indicates that the basalts were slightly earlier or coeval with initial intracontinental rifting in the Nanhua basin at ca. 820 Ma (Wang et al., 2003; Wang and Li, 2003).

Thirteen basaltic samples were collected from the Yiyang region for this study (Fig. 1). They all come from the same flow and preserve pillow structures with dimensions ranging from 0.5 to 1.5 m (Fig. 2b). Interstices between pillows are filled by tuffaceous matrix. Primary mineral textures are still preserved, although most olivine and pyroxene has been altered to tremolite, sericite, talc, and epidote (Fig. 2c, d and e). Our previous study (Wang et al., 2007) shows that all but a few highly evolved, crustally contaminated basaltic rocks are characteristically high in MgO (10.2–17.5%), Ni (183–661 ppm) and Cr (677–1672 ppm), but low in TiO_2 (0.5–0.7%), Al_2O_3 (10.6–12.7%) and FeO^T (total Fe as FeO^T, 7.4–10.5%). Geochemical modeling, which removes the effect of olivine crystallization, suggests that their primary magma was a typical komatiitic basalt with MgO = 20%, FeO^T = 11%, SiO_2 = 47%, TiO_2 = 0.48%, Al_2O_3 = 10%, Ni = 860 ppm and Cr = 1780 ppm (Wang et al., 2007). Although they underwent variable degrees of alteration, their high field strength elements (HFSE), rare earth elements (REE), Th, U, Sc, SiO_2, MgO, Al_2O_3, and FeO^T were essentially immobile during this process. This is confirmed by their relatively low LOI (loss on ignition) values (mostly < 3%).

3. Analytical methods

The sample preparation is the same as that given by Wang et al. (2007). The major and trace element data were previously reported in Wang et al. (2007). In this study, we analyzed Nd and Hf isotopes of thirteen whole–rock samples, and Re−Os isotopes of eight of these (05SC72–2, −3, −4, −6, and − 8, 05SC74–2, −4 and − 5).

Neodymium and Hf fractions were separated at the super–clean laboratory of the State Key Laboratory of Isotope Geochemistry, Guangzhou Institute of Geochemistry, Chinese Academy of Sciences (SKLaBIG, GIGCAS). Nd isotopic ratios were determined using a Micromass Isoprobe multi–collector ICPMS at GIGCAS, using procedures described by Li et al. (2004). Around 150 mg rock powder were dissolved in a high-pressure Teflon bomb for 24 h using a HF + HNO 3 mixture to ensure complete sample digestion. Samples were spiked to allow concentration determinations by isotope dilution. Sm and Nd fractions were separated by passing through cation columns followed by HDEHP columns. Samples were taken up in 2% HNO_3, and the aqueous solutions were introduced into the MC–ICPMS using a Meinhard glass nebulizer in free-aspiration mode with an uptake rate of 0.1 mL/min. The inlet system was cleaned for 5 min between analyses using high purity 5% HNO_3, followed by a blank solution of 2% HNO_3. Measured $^{143}Nd/^{144}Nd$ ratios were normalized to $^{146}Nd/^{144}Nd = 0.7219$, and the reported $^{143}Nd/^{144}Nd$ ratios were further adjusted relative to the Shin Etsu JNdi-1 standard of 0.512115, corresponding to a value of 0.511860 for the La Jolla standard (Tanaka et al., 2000).

Hf isotope was separated from separate powder aliquot. Around 100 mg of rock powder were mixed with 200 mg of $Li_2B_4O_7$ and the mixture was digested for 15 min at 1200 °C in a Pt−Au crucible. It was

then dissolved in 2 M HCl. The samples were spiked for Lu and Hf isotope dilution analyses prior to digestion. The Hf fraction was separated using a modified single-column procedure by ion exchange using Eichrom® Ln-Spec resin (Li et al., 2007b). Hf isotopes were analyzed using a ThermoFinnigan Neptune MC-ICP-MS at the State Key Laboratory of Lithospheric Evolution, Institute of Geology and Geophysics, Chinese Academy of Sciences (IGGCAS) in Beijing. The $^{176}Hf/^{177}Hf$ ratios were normalized to $^{179}Hf/^{177}Hf = 0.7325$, and then further adjusted relative to the JMC-475 standard ($^{176}Hf/^{177}Hf = 0.282160$). During the course of this study, international standard rocks BHVO-2 and JB-1 yielded $^{176}Hf/^{177}Hf = 0.283099 \pm 6$ (2 σ, n = 7) and 0.282974 ± 7 (2 σ, n = 7), respectively, which are in good agreement with the results reported by Kleinhanns et al. (2002).

The chemical separation techniques employed in this study for Re−Os analyses were described by Li et al. (2015a) and the analyses were undertaken at GISCAS. In brief, Os and Re concentrations and Os isotopic measurements were made on 2–3 g bulk powdered samples. Samples were spiked with solutions enriched in ^{190}Os and ^{185}Re and digested in inverse aqua regia in sealed Carius tubes at 230 °C for at least 24 h (Shirey and Walker, 1995). Osmium was extracted by carbon tetrachloride and subsequently extracted back into high–purity concentrated HBr (Cohen and Waters, 1996; Pearson and Woodland, 2000). Further purification of Os was accomplished via micro–distillation in a conical Teflon vial (Roy-Barman et al., 1996). The purified Os was then ready for mass spectrometry. Rhenium was separated using Bio–Rad AG 1–X8 anion exchange resin (100–200 mesh).

Osmium isotopic compositions were measured using a GV IsoProbe–T negative thermal ionization mass spectrometer (TIMS) at the IGGCAS. Four duplicate analyses were also carried out using a Thermo–Finnigan Triton TIMS at the State Key Laboratory of Geological Processes and Mineral Resources, China University of Geosciences in Wuhan. The mass spectrometric procedures used in this study followed those described by Creaser et al. (1991) and Volkening et al. (1991). The Os was loaded on high purity Pt filaments (99.999%, 1 mm × 0.025 mm, H. Cross Co. Ltd.). The sample was covered with 1 μL 10,000 ppm $Ba(NO_3)_2$ solution (CLARITAS, SPEX Inc.). Osmium isotopic compositions were measured in pulse counting electron multiplier mode. Instrumental mass fractionation of Os was corrected by normalizing the obtained $^{192}Os/^{188}Os$ ratio to 3.08271 (Nier, 1973). Oxide corrections were made using $^{17}O/^{16}O = 0.00037$ and $^{18}O/^{16}O = 0.002047$. Rhenium was determined using a Finnigan Neptune MC-ICPMS (VG Instruments, England) at IGGCAS. For Re measurements, an Aridus desolvation high-efficiency nebulizer was used for sample delivery, using Ir-doped sample solutions for controlling mass fractionation of Re through monitoring the $^{190}Ir/^{191}Ir$ ratio on line (Re and Ir ion beams were detected simultaneously in a Faraday cup). The analytical procedure is described in detail in Li et al. (2007c). During the course of this study, USGS basalt BIR-1a yielded $^{187}Os/^{188}Os = 0.13380 \pm 0.00096$ (2σ, n = 4), Os = 0.352 ± 0.41 ppb (2σ, n = 4), and Re = 0.683 ± 0. 10 ppb (2σ, n = 4), which are in good agreement with the results reported by Li et al. (2015b) and Zhang et al. (2017), as well as those of other labs (e.g. Ackerman et al., 2017).

The total blank levels for Re and Os were 5 ± 3 and 0.42 ± 0.42 pg (2σ, n = 3), respectively, which are negligible compared to their concentrations in most samples. All data were corrected for blanks.

4. Results

4.1. Nd and Hf isotopes

The Yiyang samples display fairly constant $^{143}Nd/^{144}Nd$ ratios ranging from 0.51221 to 0.51231, except for one highly evolved sample (05YY–2) with much lower $^{143}Nd/^{144}Nd = 0.51190$ (Table S1). The calculated initial $\varepsilon_{Nd}(t = 825\,Ma)$ values vary from −1.3 to −4.5. Except for one high silica sample (05YY–2) that has lower $\varepsilon_{Hf}(t)$ values of −1.1, all other samples have initial $\varepsilon_{Hf}(t)$ values of +3.0 to +4.3, corresponding to remarkably uniform $^{176}Hf/^{177}Hf$ ratios between 0.28258 and 0.28267.

4.2. Re−Os isotopes

Whole–rock Re and Os concentrations range from 0.128 to 0.384 and from 0.162 to 0.485 ppb (mostly > 0.3 ppb), respectively (Table S2). Os concentrations correlate with major (e.g. Al_2O_3, MgO and TiO_2) and trace elements (e.g. Ni, Th, and Nb) (Fig. 3). Assuming a primary melt composition of 20 wt% MgO, 10% Al_2O_3, and 860 ppm Ni (Wang et al., 2007), the correlations of MgO, Al_2O_3 and Ni versus Os (Fig. 3a, b, d) would predict 0.6 ppb Os in the primary melt. The Os concentrations of the Yiyang basalts are much higher than those of mid-ocean ridge basalts (MORBs) and arc volcanic rocks, but similar to those of ocean island basalts (OIBs) and published values for komatiites (Fig. 4a).

The $^{187}Os/^{188}Os$ ratios range from 0.153 to 0.442 (mostly between 0.271 and 0.215) and the calculated initial $^{187}Os/^{188}Os$ isotopic ratios (t = 825 Ma) range from 0.134 to 0.282, corresponding to γOs(t) values from +11 to +132 (the parameters of Os evolution curve used to calculate gamma Os values are shown in Table S2.). Sample 05SC72–2 has the highest Os concentration and the lowest $(^{187}Os/^{188}Os)_i$ (Fig. 4b). In contrast, sample 05SC72–4 has the highest $(^{187}Os/^{188}Os)_i$ and the lowest Os content (Os = 0.16 ppb) with relatively high SiO_2 (~51%) and Al_2O_3 (~14%) contents, but low MgO (~10%) content. The $(^{187}Os/^{188}Os)_i$ ratios of the Yiyang samples are negatively correlated with Os, and $Mg^{\#}$, but positively correlated with Al_2O_3, and TiO_2 (Fig. 5a, b, c and d). All the basaltic samples have Al_2O_3/TiO_2 ratios of 21–23 with flat HREE patterns (Wang et al., 2007 and Table S1), similar to those of Al–undepleted or Munro–type komatiites (Arndt, 2003; Robin-Popieul et al., 2012).

5. Discussion

5.1. Alteration, fractional crystallization and continental crustal contamination

The primary melt compositions may be influenced by post–melting processes, such as assimilation fractional crystallization (AFC) and alteration. Therefore, before discussing the melt generation process, we need to evaluate the contribution of these processes on the whole–rock geochemical compositions. According to our earlier study (Wang et al., 2007), the high field strength elements (HFSE, such as Nb and TiO_2), REE, Th, U, Sc, SiO_2, MgO, Al_2O_3 and FeO_T are essentially immobile during alteration, as shown by the good correlations between them and Zr. In this study, there is no correlation between LOI and Re/Os or $^{187}Os/^{188}Os$ ratios (Fig. 5e, f) suggesting that the Re−Os isotope system was not disturbed during later hydrothermal alteration (See Van Acken et al., 2016). Furthermore, the Os contents tightly correlate with MgO and Ni (Fig. 3a, d), possibly reflecting the contribution of olivine fractionation. However, as indicated by Gannoun et al. (2016), there is little evidence to suggest that the Os is strongly partitioned into olivine. Studies on natural basaltic olivines from different basaltic rocks (e.g. picritic lavas from Bandama, Grand Canary, less MgO rich basalts from Mt. Maletto and Mt. Silvestri on Mt. Etna, Italy and basanites from the Cameroon volcanic line) indicate that Os is highly incompatible in olivine (Burton et al., 2002; Gannoun et al., 2015). On the other hand, sulfide strongly incorporates Os, with sulfide/silicate melt partition coefficients of 10^5–10^6 (Brenan et al., 2016). Therefore, the tight correlations between Os and MgO and Ni contents can be explained by fractionation of olivine with sulfides or platinum–group element (PGE)–rich alloy phases that occur as inclusions in the olivine (e.g. Burton et al., 2002; Day, 2013). Previous studies have demonstrated

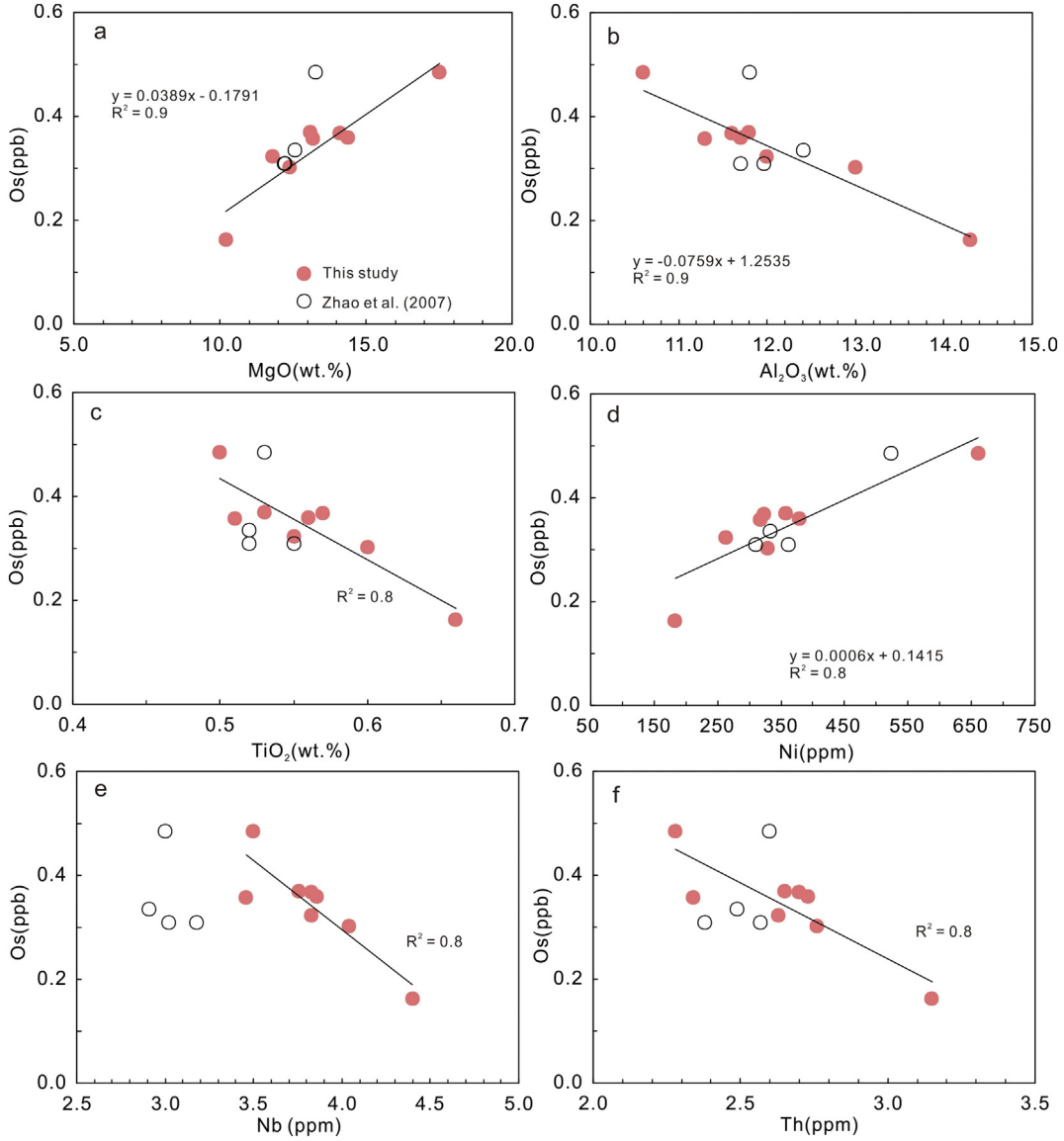

Fig. 3. Os (ppb) vs. selected major and trace elements for the Yiyang high–MgO basalt. The data of Zhao and Zhou (2013) were not used to establish the correlation coefficients, because of their high LOI. The correlations shown in (a), (b) and (d) were used to calculate the Os concentration of the primary magma.

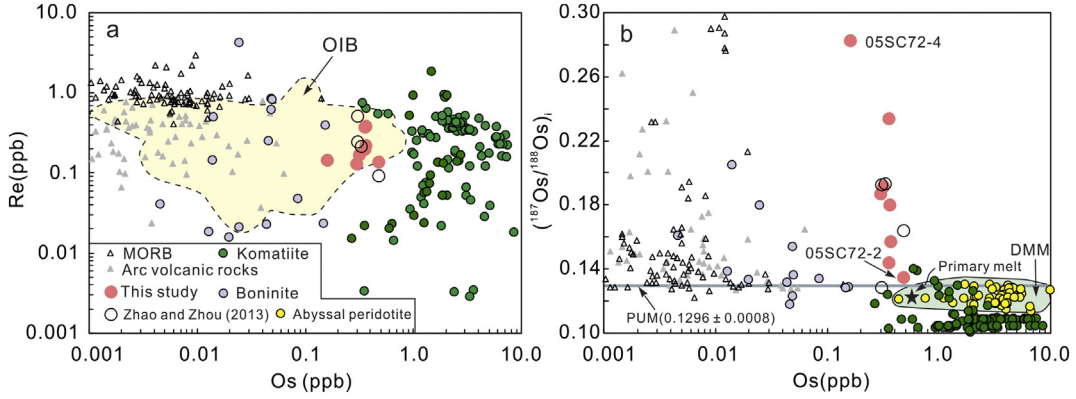

Fig. 4. (a) Plot of Re and (b) $(^{187}Os/^{188}Os)_i$ vs. Os. Data for arc volcanic rocks and MORB are from Alves et al. (2002), Turner et al. (2009), Woodhead and Brauns (2004), Escrig et al. (2005), Gannoun et al. (2015), and Lissner et al. (2014). Data for boninites are from Suzuki et al. (2011) and Senda et al. (2016). The OIB field is from Shirey and Walker (1998). Data for komatiites are from Brandon et al. (2003), Puchtel et al. (2004, 2005, 2009, 2014), Connolly et al. (2011) and Van Acken et al., 2016. PUM in (b) indicates putative present–day primitive upper mantle with $^{187}Os/^{188}Os = 0.1296 \pm 0.0008$ (Meisel et al., 2001). The light green area represents the range of depleted mid-oceanic-ridge basalt (MORB) source mantle (DMM) estimated from abyssal peridotite (Liu et al., 2008 and Harvey et al., 2006). (For interpretation of the references to color in this figure legend, the reader is referred to the web version of this article.)

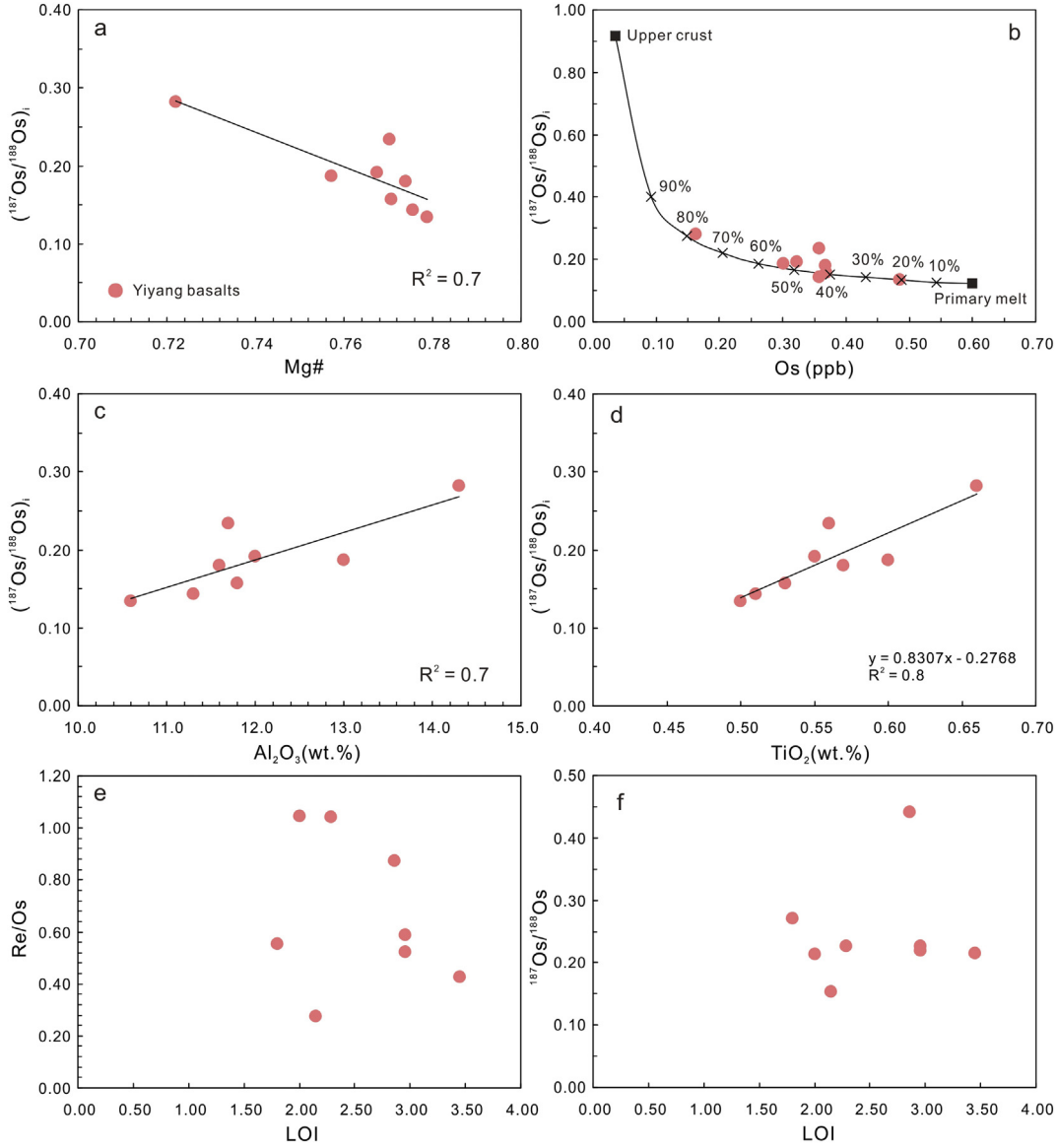

Fig. 5. (a), (b), (c) and (d) Correlations between $(^{187}Os/^{188}Os)_i$ and major and trace elements. The two end–members (see text for details) in (b) were chosen for modeling. (e) and (f) Re/Os and $^{187}Os/^{188}Os$ vs. LOI diagrams.

that Cu is incompatible in olivine ($D_{ol/melt}$ = 0.05), orthopyroxene (0.035), clinopyroxene (0.04), amphibole (0.05), garnet (0.004), and spinel (0.2), but is strongly partitioned into sulfide minerals ($D_{sf/melt}$ = 600–1200) (Lee et al., 2012). Therefore, the decreasing Cu with increased SiO_2 and decreased Mg# values suggested these basalts are sulfide saturated (figures not shown). As shown in Fig. 6a, 4–21% fractionation of olivine +0.001% sulfide can explain the Os—Ni variation of the Yiyang basalts. However, several lines of evidence argue that fractional crystallization alone cannot explain the observations.

Firstly, if produced solely by olivine fractional crystallization, the MgO variations (from 18% in 05SC72–2 to 10% in 05SC72–4) would require about 25% fractional crystallization of olivine with Fo = 90 (Fo = 100 * Mg/(Fe + Mg), molar ratios in olivine), whereas the SiO_2 (47–54%) and Al_2O_3 (11–15%) variations predict a very high proportion of olivine fractional crystallization (up to 60% for SiO_2) (Fig. 6b, c, d). Secondly, their Os concentrations are strongly correlated with not only compatible elements (e.g. MgO and Ni; Fig. 3a, d) but also with highly incompatible elements (e.g. Nb, Th and La; Fig. 3e, f and Fig. 6e), as well as incompatible element ratios such as Nb/U (Fig. 6f). Because such incompatible element ratios are insensitive to fractional crystallization of olivine, their concentrations can only be strongly affected by contamination by continental crust or mixing of distinctive melts. Thirdly, the large FeO_T variations (5–11%) are also inconsistent with fractional crystallization of olivine, because the partition coefficient of Fe between olivine and melt is close to unity (Putirka, 2005). Although significant crystallization of plagioclase plus olivine could result in large FeO_T variations, such a process would produce a negative correlation between MgO and FeO_T (Herzberg et al., 2007), whereas the opposite trend was observed (figure not shown). Therefore, the co–variations mentioned above are mainly attributed to contamination or mixing processes rather than simple fractional crystallization.

Some continental crustal contamination is inevitable when basaltic lavas pass through the Earth's crust. Because of its very high liquidus temperature, low viscosity and low incompatible element contents, komatiitic melt is especially susceptible to contamination by continental crustal rocks (e.g. Arndt and Jenner, 1986; Huppert et al., 1985; Puchtel et al., 1997). In the case of the Yiyang basalts, our earlier studies have shown that crustal contamination played an important role during magma evolution, because negative correlations between FeO_T/MgO, SiO_2/MgO and Nb/La with Nb/U ratios were observed (Wang

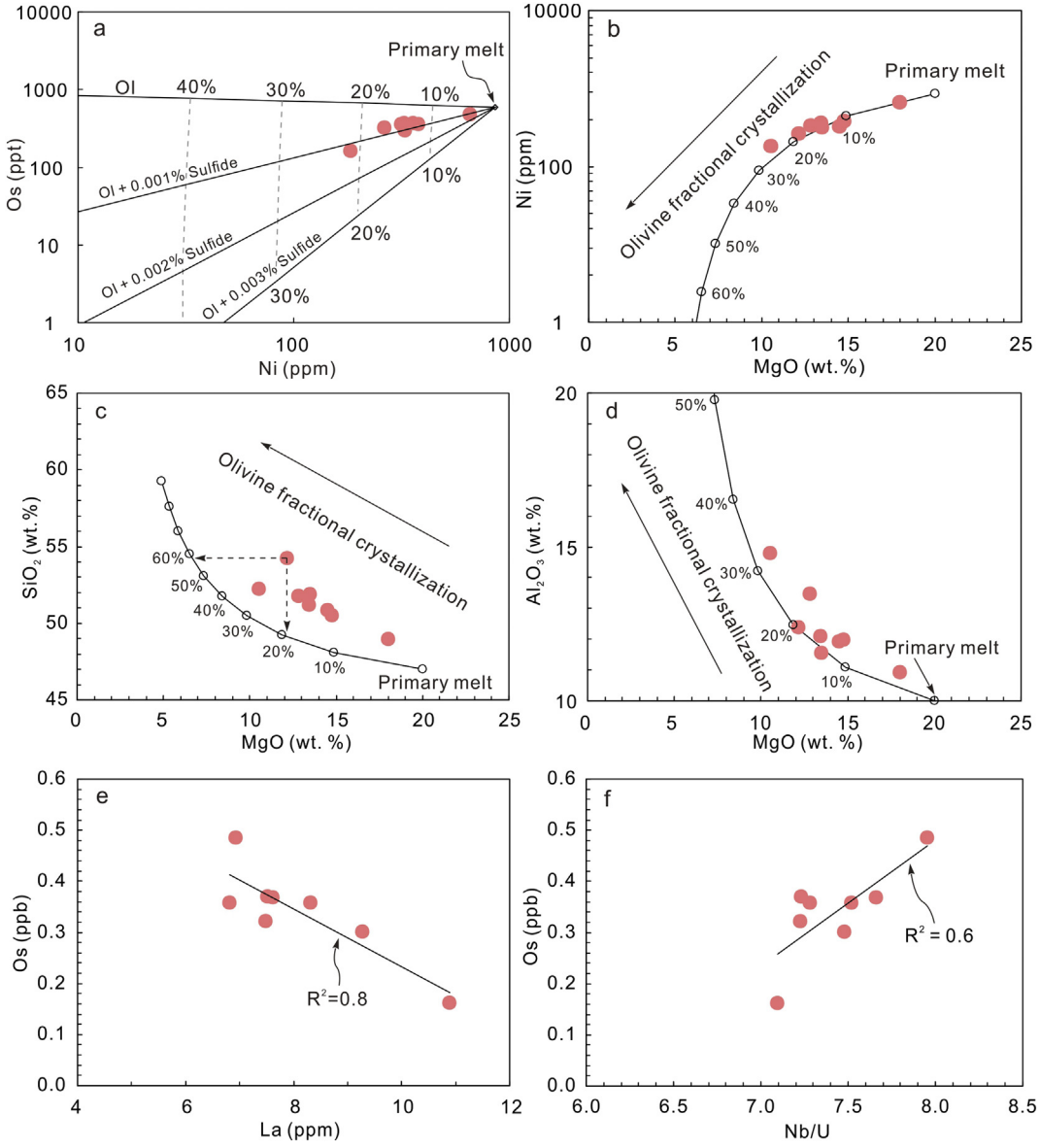

Fig. 6. (a) fractionation of 4–21% olivine + 0.001% sulfide can explain the Os—Ni variation in the Yiyang basalts. The primary melt was assumed to have Ni = 860 ppm and Os = 0.6 ppb. The D_{Ni} and D_{Os} between olivine and melt is 7.4 and 0.51, respectively (Burton et al., 2002). The D_{Ni} and D_{Os} between sulfide and melt is 600 and $5 * 10^5$, respectively (Burton et al., 2002; Brenan et al., 2016). Fractionation of olivine in (b) 4–21%, (c) 20–60%, and (d) 10–32% can model the MgO, SiO_2 and Al_2O_3 contents of the Yiyang basalts. The D_{MgO}, D_{SiO2} and D_{Al2O3} between olivine and melt are from Beattie (1994). (e) La and (f) Nb/U show good correlations with Os. Primary melt: MgO = 20%, SiO_2 = 47%, Al_2O_3 = 10%, Ni = 860 ppm (Wang et al., 2007) and Os = 0.6.

et al., 2007). In this present study, the broad negative correlations between $(^{187}Os/^{188}Os)_i$ ratios, $\varepsilon_{Nd}(t)$, $\varepsilon_{Hf}(t)$ and Os, Nb/La, and Th/Nb also suggest that crustal contamination occurred (Fig. 7). The least radiogenic sample (05SC72–2) has an initial $^{187}Os/^{188}Os$ values of 0.134. However, it may also have undergone crustal contamination and its Os isotopic ratio only provides the upper limit of its source. Here, we estimated the $(^{187}Os/^{188}Os)_i$ ratios of the primary magma by using the regression approach. From the correlation shown in Fig. 5d, 0.48% TiO_2 (Wang et al., 2007) in the primary magma would predict a depleted MORB mantle (DMM)-like $(^{187}Os/^{188}Os)_i$ ratio of 0.122. In the following part, we will evaluate the effect of crustal contamination on both Os isotopes and trace elements of the Yiyang basalts.

The Yiyang basalts are characterized by relatively high Os concentrations (up to 0.485 ppb), suggesting this is not the result of upper crustal contamination, because possible highly radiogenic upper crustal materials have very low Os contents (0.036 ± 0.008 ppb; $^{87}Os/^{188}Os$ (t = 825 Ma) = 0.916; Chen et al., 2016). To develop such radiogenic Os isotopes, simple mixing of 20–80% of a hypothetical 825 Ma crustal component (Chen et al., 2016) into a primary Yiyang basalt melt (Os = 0.6 ppb; $(^{187}Os/^{188}Os)_i$ = 0.122) would be required to reproduce the $(^{187}Os/^{188}Os)_i$ variation (Fig. 5b). However, such high and variable degrees of crustal contamination are inconsistent with the high MgO and FeO contents of the Yiyang samples. The nearly constant Hf—Nd isotopes of the least–evolved samples also preclude the possibility of high and variable degrees of UCC contamination (Table S1). Furthermore, assuming that olivine + 0.001% sulfide are the only fractionating phases, upper crustal assimilation and fractional crystallization (AFC) simulation suggests that when Os > 0.1 ppb, the $(^{187}Os/^{188}Os)_i$ ratios change very little, failing to simulate the geochemical variations seen in the Yiyang basalts (Fig. 8a). Therefore, upper crustal materials seem to have played an insignificant role in the Re—Os isotope diversity of the Yiyang basalts. This being the case, it is necessary to test whether lower crustal material may have contributed to the mafic magmas.

The Re and Os contents of lower continental crust (LCC) are quite

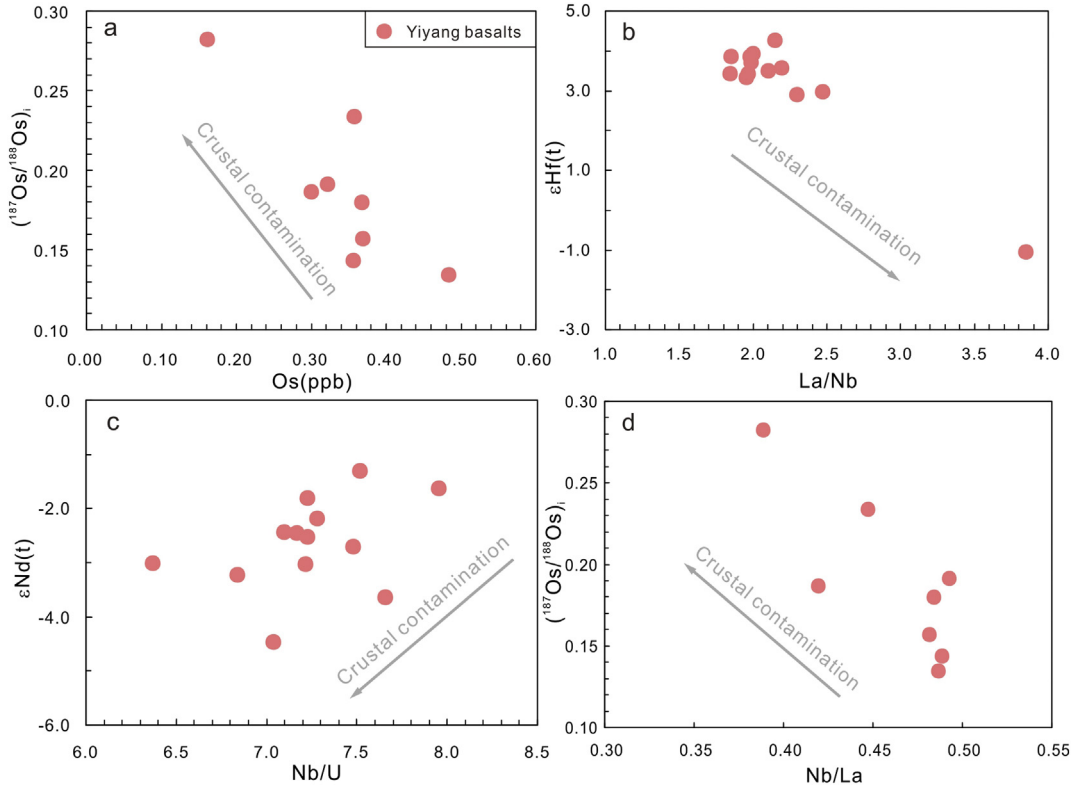

Fig. 7. Plots of (a) $(^{187}Os/^{188}Os)_i$ vs. Os; (b) $\varepsilon_{Hf}(t)$ vs. La/Nb; (c) $\varepsilon_{Nd}(t)$ vs. Nb/U; (d) $(^{187}Os/^{188}Os)_i$ vs. Nb/La. All figures show crustal contamination may have occurred.

heterogeneous. According to the limited lower crustal xenolith data that are available, the LCC has Re and Os contents ranging from 0.0345 to 1.21 ppb and from 0.0032 to 1.043 ppb, respectively (Saal et al., 1998). Here, we use a Re concentration of 0.5 ppb as the value of the lower crust beneath the SCB. Previous studies have demonstrated that the Archean TTG gneisses of the Kongling Complex, which are considered as the basement rock in our study area, were mainly emplaced at 3.0–2.9 Ga and metamorphosed at 2.73 Ga and 2.0 Ga (Zhao and Cawood, 2012 and references therein). We use 2.9 Ga as the likely mean age for the lower crust and use Os concentrations of 0.01, 0.03, 0.05 and 0.1 ppb, respectively, to calculate the $^{187}Os/^{188}Os$ ratios at 825 Ma. We then conducted AFC modeling by assuming that olivine +0.001% sulfide are the only fractionating phases. As shown in Fig.8b, a LCC AFC model can account for the Ni concentrations and Os isotope variations of the Yiyang basalts.

However, the Yiyang basalts have low Nb/La (0.4–0.5; upper crust: Nb/La = 0.4; lower crust = 0.6; Rudnick and Gao, 2003) and Nb/Th (1.4–1.5; upper crust: Nb/Th = 1.1; lower crust = 4.2; Rudnick and Gao, 2003) ratios. If such elemental ratios were caused by the upper crustal contamination, it would require > 70% crustal materials to have contaminated the magma (Fig. 8c). Such high degrees of crustal contamination are inconsistent with the high MgO and low SiO_2 signatures of the Yiyang samples (Table S1). Low crustal contamination also failed to explain the geochemical variation of the Yiyang basalts (Fig. 8c). Therefore, it seems that crustal contamination cannot account for the enrichment in LREE and large-ion lithophile elements (LILE) relative to HFSE in the Yigang basalts, indicating they were most likely inherited from the primary source.

5.2. Are they boninites?

As mentioned earlier, along with the Yiyang basalts, there are also several other contemporary (ca. 830 Ma) high–MgO pillow lavas, such as the Sibao, Lushan, Shexian and Zhangyuan high–MgO basalts within the early Neoproterozoic strata in the central SCB (Fig.1). Zhao and Asimow (2014) proposed they were generated within a subduction setting. Previously, the Yiyang basalts from the central SCB were considered to be typical plume related high–MgO lavas (e.g. Xiao, 1988; Wang et al., 2007; Che et al., 2005). In our earlier study (Wang et al., 2007), it was demonstrated that the Yiyang lavas have relatively low SiO_2, negatively sloping REE patterns, high Th/U, Ti/V and Ti/Sc ratios, and high Ni contents, which are distinct from typical subduction–related high–MgO mafic rocks, i.e. boninites. However, in subsequent studies, Zhao and Zhou (2013) and Zhao and Asimow (2014) proposed that the ca. 830 Ma high–MgO volcanic rocks in the central SCB were typical boninite–series rocks.

Boninites are volcanic rocks derived from shallow partial melting of highly–depleted hydrous mantle, fluxed with water from subducted slabs. They are mafic lavas with high SiO_2 (> 52 wt%) and MgO (> 8 wt%), but with TiO_2 as low as < 0.5 wt% (Le Bas, 2000). Compared with typical boninites, the data for the published ca. 830 Ma high–MgO volcanic rocks in the central SCB have lower SiO_2 contents (average SiO_2 = 51.3 wt%; N = 77), and lower Al_2O_3/TiO_2 (average Al_2O_3/TiO_2 = 21; N = 77; boninites: average Al_2O_3/TiO_2 = 57; N = 573) ratios. However, they have higher TiO_2 (average TiO_2 = 0.74; N = 77; boninites: average TiO_2 = 0.3; N = 575), Zr (43.6–198 ppm; boninites: average Zr = 27 ppm; N = 456), Nb (2.5–8.4 ppm; boninites: average Nb = 1.8 ppm; N = 321), and Nd (up to 25.6 ppm; boninites: average Nd = 2.9 ppm; N = 316) contents and Th/U ratios (3–7; boninites: average Th/U = 2.5 ppm; N = 179) (Fig. 9) than boninites, and therefore, almost all of them plot outside of the field of typical boninites (Fig. 9a, c; Le Bas, 2000). As shown in Fig. 9a, these rocks have geochemical compositions that are mostly distinct from those of typical boninites from Tonga and Troodos (Golowin et al., 2017). Additionally, boninites normally have negative Nb−Ta and Ti anomalies (unusually low concentrations) and positive Rb, Ba, and Sr anomalies in mantle–normalized trace element distribution patterns (Crawford et al., 1989; Arndt, 2003). Their REE

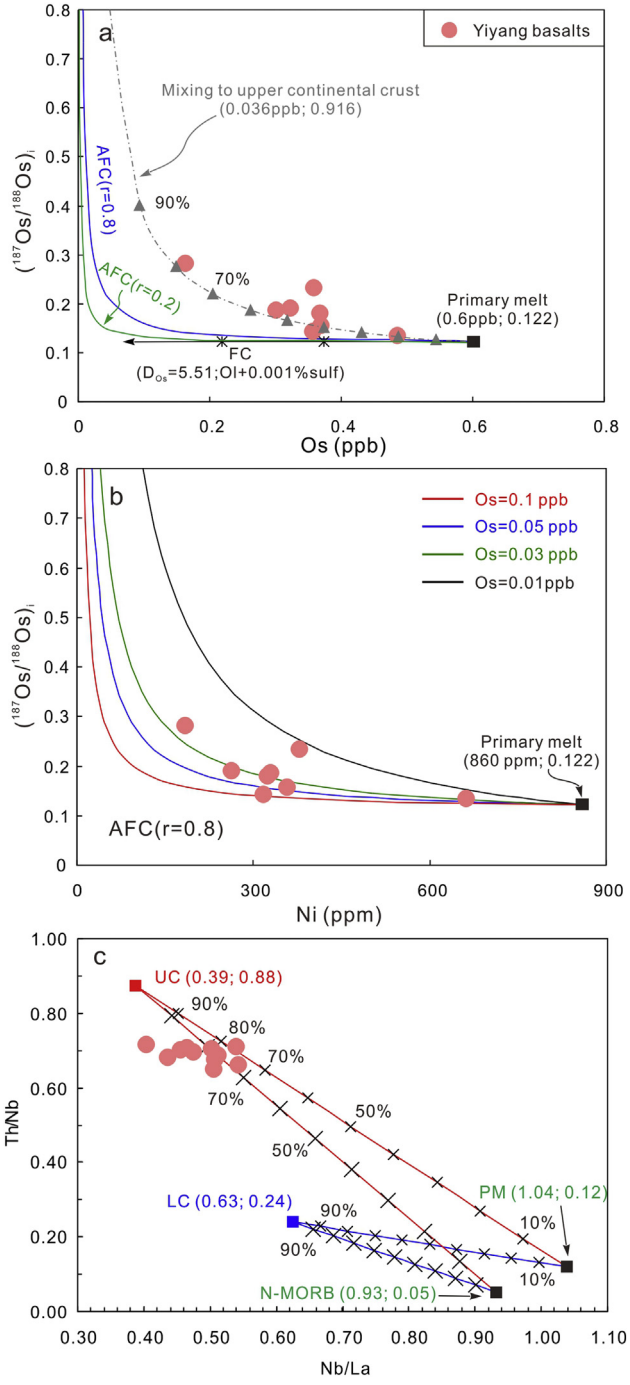

Fig. 8. (a) and (b) AFC models (DePaolo, 1981) for the Yiyang basalts; (c) Th/Nb vs. Nb/La diagram. Primary melt: $(^{187}Os/^{188}Os)_i$ = 0.122; Os = 0.6 ppb. Upper crustal materials in (a): $(^{187}Os/^{188}Os)_i$ = 0.916; Os = 0.036 ppb (Chen et al., 2016). Lower crustal materials in (b) (see text for details). In (a), simple bimodal mixing (the dashed line) and fractional crystallization models (horizontal line with arrow) are also shown. r = Ma/Mc; where Ma is the amount of assimilated material and Mc is the amount of crystallized material. Upper crust (UC) and Lower crust (LC) in (c) are from Rudnick and Gao (2003). Primitive Mantle (PM) and N-MORB are from Sun and McDonough (1989).

patterns commonly have a characteristic U shape, due to low concentrations of the middle REE (MREE) compared to the light REE (LREE) and heavy REE (HREE) (Arndt, 2003). However, most of the ca. 830 Ma high–MgO basalts in the central SCB have negative Ba and Sr anomalies with depleted HREE patterns, which are distinct from those of typical boninites from Cape Vogel, Papua New Guinea and the Izu–Bonin–Mariana arc (Fig.10). Additionally, the relatively high melting pressure of the Yiyang basalts (up to 3.0 GPa; Wang et al., 2007) further argues against the boninite model, because boninites form at relatively shallow depths (ca. 30–50 km, Crawford et al., 1989).

Furthermore, boninites are commonly considered to be the result of melting of highly–depleted (through previous melt extraction) peridotitic mantle, triggered by addition of a hydrous slab–derived fluid or melt enriched in incompatible elements (Crawford et al., 1989; Sobolev and Danyushevsky, 1994).The peridotitic source of boninites will be highly susceptible to modification by melts and fluids passing through them. Many studies of mantle wedge peridotites have reported that most have highly radiogenic Os isotopes (Brandon et al., 1996; Widom et al., 2003). As a consequence, like other arc basalts (e.g. Alves et al., 1999; Borg et al., 2000; Woodhead and Brauns, 2004; Righter et al., 2008), boninites may also have radiogenic Os isotopic compositions with low Os concentrations (e.g. Suzuki et al., 2011; Senda et al., 2016). From this study, the primary melt of the Yiyang basalts most likely had high Os concentration (0.6 ppb), coupled with DMM–like Os isotopes ($(^{187}Os/^{188}Os)_i$ = 0.122), such features being similar to those of komatiites, and thus were unlikely to have been generated by water–-fluxed melting of an ultra–depleted peridotite source, as required for boninites (Fig. 4b).

One of the key pieces of evidence cited to support an arc origin for these ca. 830 Ma high–MgO basalts was their enrichment of LREE and LILE relative to HFSE in the primitive mantle normalized trace element diagrams, i.e. the so–called “arc signatures” (Zhao and Zhou, 2013; Zhao and Asimow, 2014). However, Wang et al. (2016) demonstrated that such “arc signatures” are also present in many large intraplate igneous provinces, such as Karoo, Siberia, CAMP (Central Atlantic magmatic province), Columbia River, Emeishan, and Deccan (e.g. Luttinen et al., 1998; Xiao et al., 2004; Shirey et al., 1994; Wang et al., 2016; Ivanov et al., 2018). They further pointed out that Ti—V and Zr–Zr/Y discrimination diagrams can effectively distinguish arc–like intra–continental basalts from true arc basalts. Here, only samples with $SiO_2 \leq 56\%$ (volatile–free) of the ca. 830 Ma high–MgO basalts in the central SCB were used (Fig. 11). Samples from Yiyang, Zhuangyuan, Shexian and Sibao mostly plot near the boundary between arc tholeiite and MORB (Fig. 11a), whereas those from Lushan plot in or near the MORB fields (Fig. 11a). Nearly all samples plot outside of the IAB field (Fig. 11b). Considering their close spatial and temporal relationships, we suggest that they were most probably generated within an intraplate setting rather than a subduction environment. There are also many geological observations that support this conclusion: 1) The ca. 830 Ma high–MgO magmatism was slightly earlier to almost coeval with initial intracontinental rifting in the Nanhua Basin at ca. 820 Ma (Wang et al., 2003; Wang and Li, 2003) and the basalts were all distributed within this basin (Fig. 1); 2) Detrital zircon studies indicate that sediments across the mid–Neoproterozoic unconformity share similar sedimentary provenances and were deposited within a similar tectonic setting. Both the Sibao and Danzhou groups were most likely deposited in a continental rift basin, strongly arguing against an orogenic origin for the regional mid–Neoproterozoic unconformity between them (Yang et al., 2015); 3) The widespread ca. 825–760 Ma basaltic rocks in the SCB have continental intraplate geochemical signatures (Wang et al., 2009 and references therein); 4) The recognized ca. 870–700 Ma low–$\delta^{18}O$ magmatism in the SCB (Wang et al., 2011; Yang et al., 2015) indicates intensive high-temperature water-rock interaction, consistent with generation in a rift setting during this period; 5) New geophysical data clearly show that the Yangtze Block has a typical rifted middle–lower continental crustal structure (Dong et al., 2013, 2015). Based on all the evidence above, we propose that the ca. 830 Ma high–MgO basalts in the central SCB were most likely generated within an intraplate setting and that they cannot be classified as boninites.

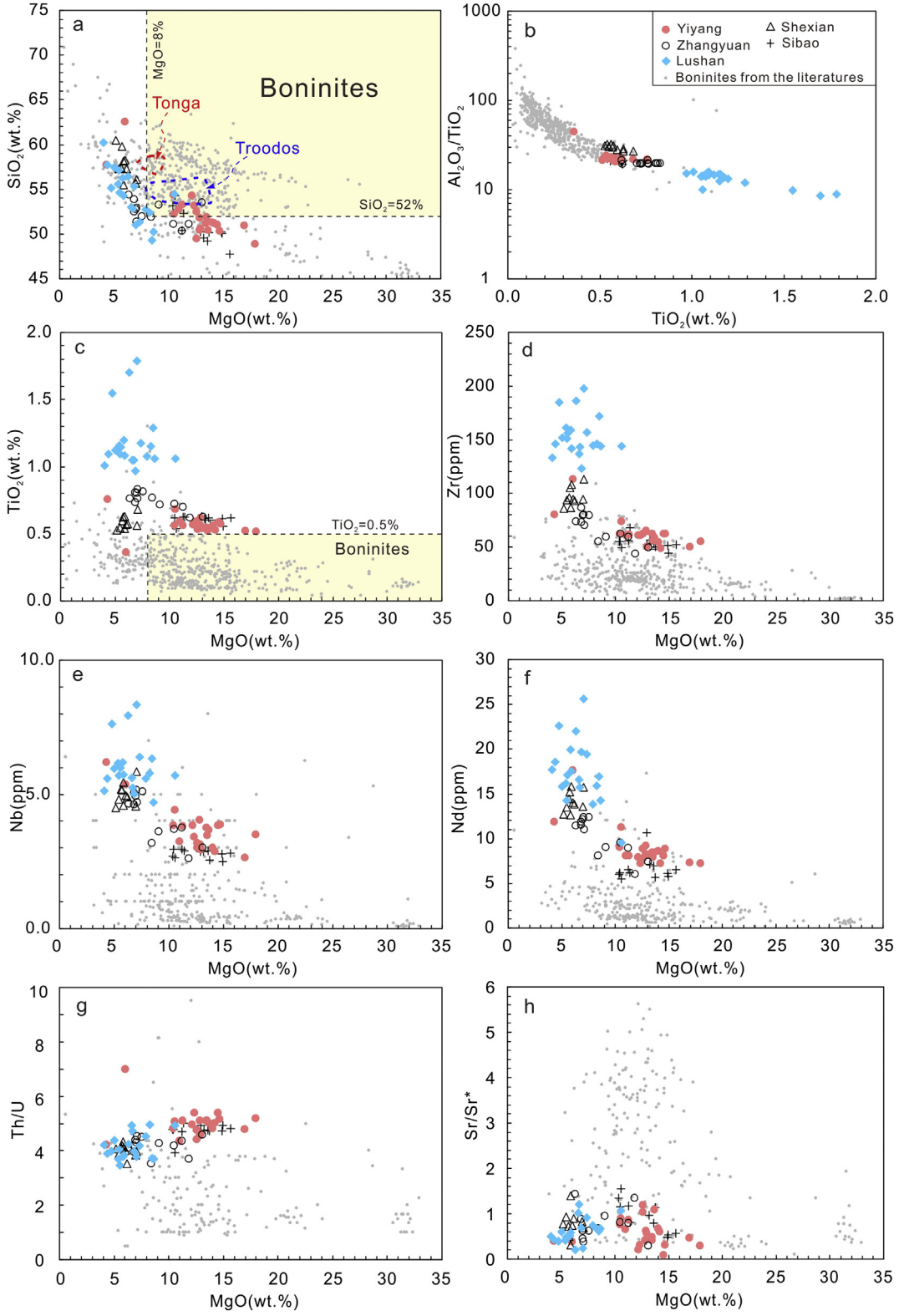

Fig. 9. Plots of (a) SiO_2, (b) Al_2O_3/TiO_2, (c) TiO_2, (d) Zr, (e) Nb, (f) Nd, (g) Th/U, and Sr/Sr* vs. MgO of the ca. 830 Ma high–MgO volcanic rocks from the central SCB and published boninites. All the data were normalized on a volatile–free basis to 100%. The fields of the Tonga and Troodos boninites are from Golowin et al. (2017) and references therein. The data for ca. 830 Ma high–MgO volcanic rocks are from Wang et al. (2007), Zhao and Zhou (2013) and Zhao and Asimow (2014). Boninite data are from http://georoc.mpch-mainz.gwdg.de/georoc/Start.asp. Only samples with LOI values ≤ 5 wt% (or total summations ranging from 95 wt% to 102%, if LOI values were not available) were considered.

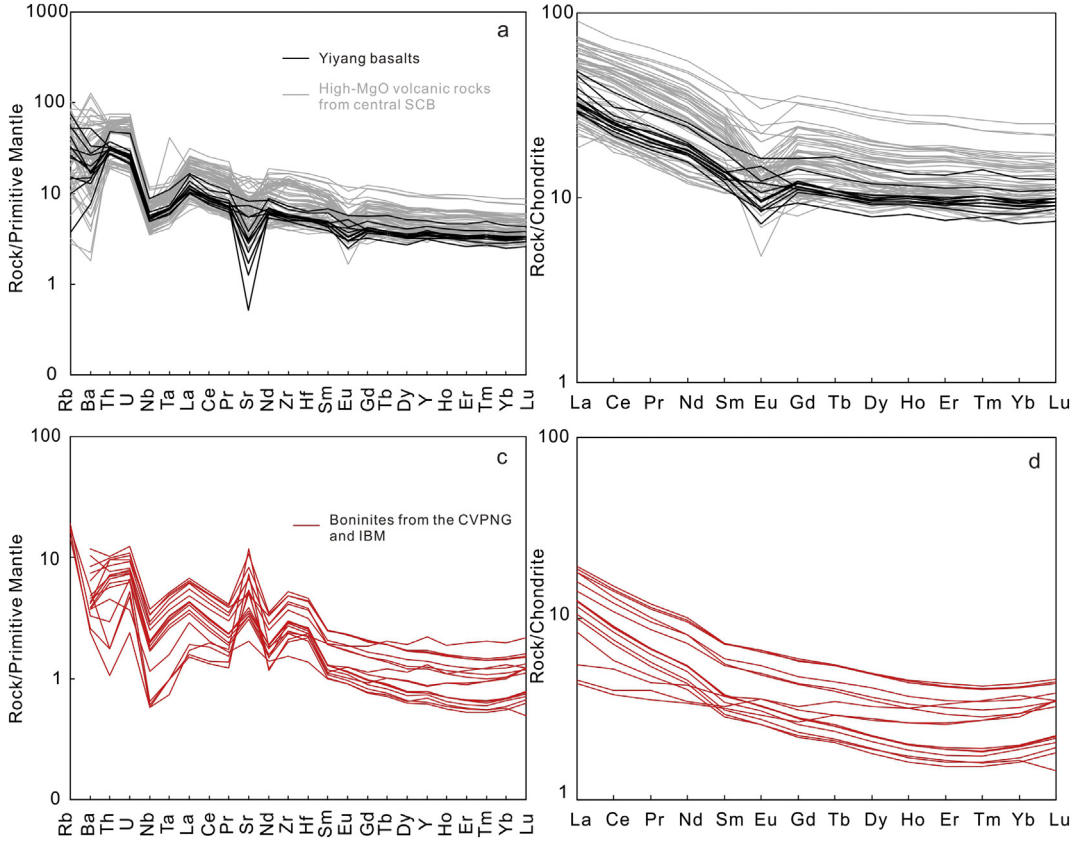

Fig. 10. (a) and (c) Primitive–mantle normalized trace element diagrams and (b) and (d) chondrite–normalized REE diagrams of the ca.830 Ma high–MgO volcanic rocks from the central SCB, and boninites from Cape Vogel, Papua New Guinea (CVPNG) and Izu–Bonin–Mariana (IBM). Typical boninites have positive Sr anomalies and u–shaped REE patterns, whereas those of the ca. 830 Ma high–MgO volcanic rocks do not. Chondrite and primitive mantle–normalized values are from Sun and McDonough (1989). The boninites from CVPNG and IBM are from Konig et al. (2010), Taylor et al. (1994), and Reagan et al. (2010).

5.3. Recycled sediments in the Yiyang mantle source

The least–evolved samples of the Yiyang basalts display high $\varepsilon_{Hf}(t)$ values relative to the Hf—Nd isotopic terrestrial array at a given Nd isotopic composition (Fig.12a; e.g. Blichert-Toft et al., 1999). Therefore, the decoupling between Hf and Nd isotopes seen in the Yiyang basalts is a primary feature of their mantle source. This distinctive isotopic fingerprint suggests that their mantle source had low time–integrated Sm/Nd and high time–integrated Lu/Hf ratios. In the upper mantle source region, the minerals that control Lu/Hf and Sm/Nd ratios during partial melting are clinopyroxene or, more effectively, garnet. The published data sets (the GERM database http://earthref.org/GERM/) indicate that clinopyroxene and garnet partition coefficients for Sm and Lu are greater than those for Nd and Hf. As a consequence, a clinopyroxene or garnet cumulate would evolve over time to positive values of both ε_{Nd} and ε_{Hf} (Blichert-Toft et al., 2015). The least–evolved sample of Yiyang basalts still has a negative $\varepsilon_{Nd}(t)$ value (05SC72–2; $\varepsilon_{Nd}(t) = -1.6$), which is inconsistent with the clinopyroxene or garnet cumulate model. Furthermore, decoupled Hf—Nd isotopes have also been observed in some other komatiites, where it was proposed to be related to the presence of recycled sediments in the source (Blichert-Toft et al., 2015). Such a scenario seems likely to have occurred in the

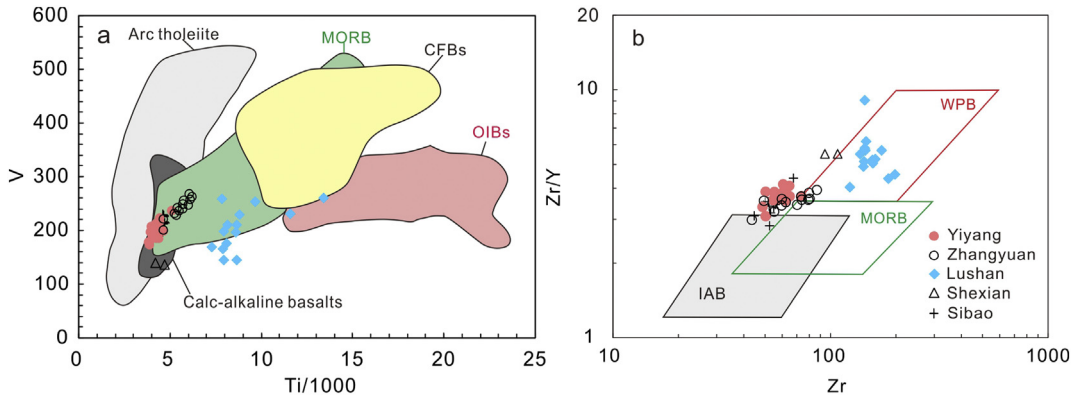

Fig. 11. Plots of (a) V vs. Ti/1000 (Shervais, 1982) and (b) Zr/Y vs. Zr (Pearce and Norry, 1979). Fields of arc tholeiitic basalts, calc-alkaline basalts, MORB, continental flood basalts (CFBs), Oceanic Island basalts (OIBs), Within Plate basalts (WPB) and Island Arc basalts (IAB) are after Wang et al. (2016). Only basaltic samples with $SiO_2 \leq 56\%$ (volatile–free) are plotted. Data source: Wang et al. (2007), Zhao and Zhou (2013) and Zhao and Asimow (2014).

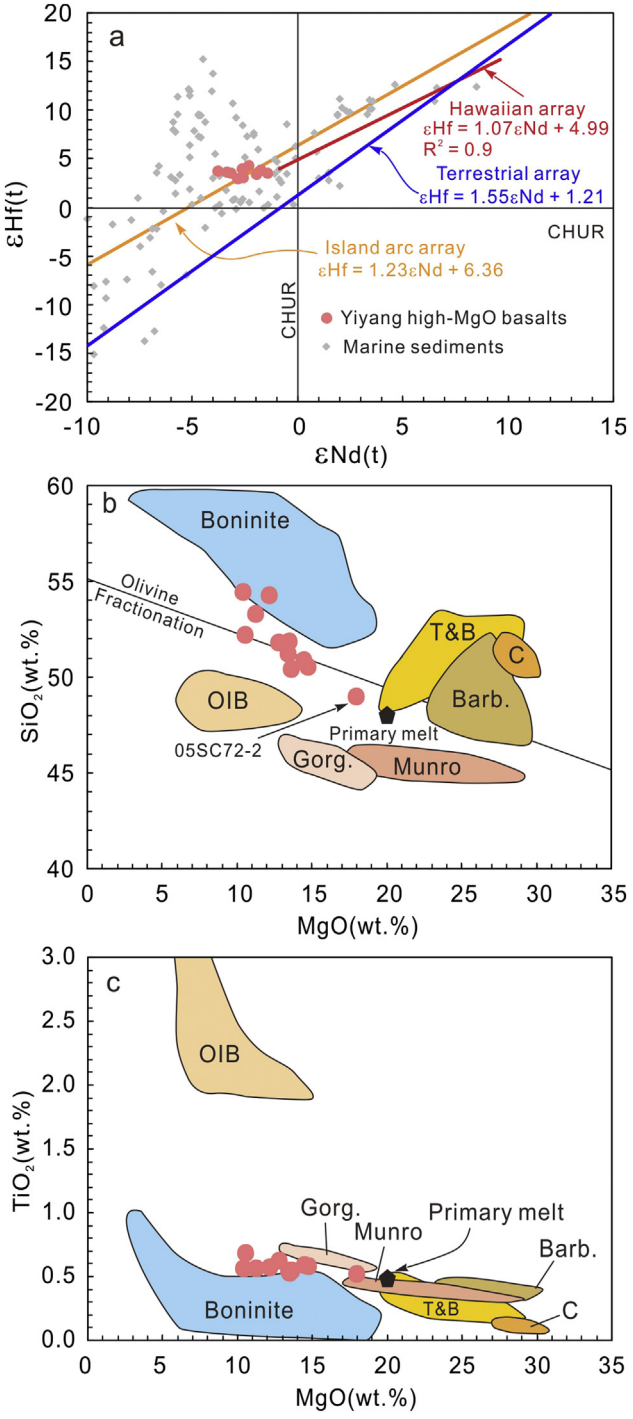

Fig. 12. (a) Plot of $\varepsilon_{Hf}(t)$ vs. $\varepsilon_{Nd}(t)$ for the Yiyang basalts. The terrestrial array is from Vervoort et al. (2011). The data for Hawaiian ocean island basalts are from Blichert-Toft et al. (1999). The data for marine sediments are from Vervoort et al. (2011). The boninite data are from Konig et al. (2010), Reagan et al. (2010) and Todd et al. (2012), and the island arc array is from Chauvel et al. (2009). (b) SiO_2 vs. MgO and (c) TiO_2 vs. MgO show that the primary melt of the Yiyang basalts was similar in composition to the 2.7 Ga Tisdale and 2.9 Ga Ball komatiites of Canada, but distinct from boninites. The fields of OIB, boninite and komatiite are from Grove and Parman, 2004. Komatiites: Barb. (Barberton, South Africa, 3.5 Ga; Parman et al., 2004), C (Commondale, South Africa, 3.3 Ga; Wilson, 2003), T (Tisdale, Canada, 2.7 Ga; Fan and Kerrich, 1997), B (Ball, Canada, 2.9 Ga; Hollings et al., 1999), Munro (Munro, Canada, 2.7 Ga; Fan and Kerrich, 1997) and Gorg. (Gorgona, South America, 0.088 Ga; Aitken and Echeverria, 1984).

case of Yiyang basalts.

Zircon grains have low Lu/Hf and $^{176}Lu/^{177}Hf$ ratios and show enrichment in Hf. Because of their "zircon effect", recycled sediments can form a distinctive isotopic reservoir that results in decoupling of the Hf and Nd isotopic systems (Vervoort et al., 1999). These sediments are characterized by high Lu/Hf ratios because zircons have been removed and thus have higher positive $\varepsilon_{Hf}(t)$ values relative to the Hf–Nd isotopic mantle array at any given Nd isotopic composition (e.g. Blichert-Toft et al., 1999; Chauvel et al., 2008). On the other hand, the Yiyang basalts plotted above the terrestrial array, close to the Hawaiian and island arc arrays (Fig. 12a). The Hawaiian and island arc arrays are shallower than the terrestrial array, which has been explained due to the presence of recycled sediments in the mantle source (Blichert-Toft et al., 1999; Chauvel et al., 2009). Additionally, the recycled components may react with mantle peridotite to form the pyroxenites (Sobolev et al., 2007), and this may be true for the Yiyang mantle source. The published data show that pyroxenites have highly variable $\varepsilon_{Hf}(t)$ (−8.5 to 65.9) and $\varepsilon_{Nd}(t)$ values (−8.3 to 27.4), and $^{187}Os/^{188}Os$ ratios (0.1264 to 2.472) (Pearson and Nowell, 2004; van Acken et al., 2010; Ackerman et al., 2016). However, as alteration and AFC process have significantly modified the whole–rock compositions of the Yiyang basalts, we cannot determine whether or not the recycled components occurred as pyroxenite in the Yiyang mantle source. Nonetheless, our new Nd–Hf data suggest that recycled oceanic sediments may have been incorporated into the source of the basalts.

5.4. Petrogenesis of the Yiyang komatiitic basalts

Mantle potential temperature (T_p) is a useful parameter for constraining thermal anomalies of the upper mantle (e.g. Herzberg and Asimow, 2008). The T_p of the Yiyang basalts was previously estimated by several different authors. Although using the same data, Wang et al. (2007) and Zhao and Zhou (2013) obtained different T_p values (> 1500 °C; Wang et al., 2007; 1444–1480 °C; Zhao and Zhou, 2013) based on their different views of the MgO content of the primary magma. For example, Zhao and Zhou (2013) used the software PRIMELT2 to calculate the composition of the primary magma (Herzberg and Asimow, 2008). They suggested that the Yiyang primary magma had much lower MgO contents (14.4–15.8 wt%) and therefore T_p values (1444–1480 °C) than was estimated by Wang et al. (2007). However, their simulation can be questioned. Firstly, the Yiyang samples had undergone some degree of alteration, with most olivine and pyroxene converted into tremolite, sericite, talc, and epidote (Wang et al., 2007). Although, as discussed above, elements like SiO_2, TiO_2, and Al_2O_3 etc. may be unaffected, however, highly mobile components like CaO, K_2O and Na_2O may be lost during alteration. Therefore, the mobile components cannot be used to estimate the primary magma composition. Secondly, crustal contamination may have modified the chemical composition, and the three samples they used (05SC72–8 ($\gamma Os(t)$ = 92), 05SC74–5 ($\gamma Os(t)$ = 48) and 05SC74–7) are amongst the most evolved, and so their primary melts were likely modified by AFC processes (see section 5.1). Therefore, the primary magma compositions calculated based on these evolved samples are suspect. Our earlier study demonstrated that the lack of correlation between phenocryst proportions and MgO concentrations rules out the possibility of olivine accumulation (Wang et al., 2007). Therefore, the primary MgO contents of the basalts may be higher than that of the least–evolved sample (18 wt%; volatile–free). Furthermore, Wang et al. (2007) used the models of McKenzie and Bickle (1988), Langmuir et al. (1992), Putirka (2005) and Herzberg et al. (2007) to calculate the T_p values considering the least–evolved sample (05SC72–2). Here, our new Os–Hf–Nd data have also shown that the primary melt of these Yiyang basalts is similar to the 2.7 Ga Tisdale, Munro and 2.9 Ga Ball komatiites of Canada, but distinct from boninites (Fig. 12b, c). Additionally, the source of komatiite has widely been considered to have close to chondritic values (Arndt et al., 2008; Puchtel et al., 2009). As we discussed above, the primary magma of the

Yiyang basalts may also have a chondritic $(^{187}Os/^{188}Os)_{i=825\ Ma}$ ratio of 0.122, which suggests that their source may be similar to those of typical komatiites. Consequently, we agree with Wang et al.'s (2007) results that the Yiyang lavas are komatiitic basalts and their T_p values are 260 ± 50 °C hotter than the contemporary ambient MORB–source mantle.

Besides the ca. 825 Ma Yiyang komatiitic basalts of this study, the Gorgona komatiites (90 Ma) are the only true komatiite formed since the Neoproterozoic (Kerr, 2005). They have high Al_2O_3/TiO_2 ratios (20–50), depleted upper mantle–like Nd isotope compositions, and were inferred to have formed from a primary magma containing about 18 ± 3 wt% MgO (Kerr, 2005; Arndt et al., 2008). Incompatible elements are strongly depleted in the Gorgona komatiites and they were proposed to have formed by dynamic melting at an average pressure of 3–4 GPa, leaving residual harzburgite (Kerr, 2005). In this study, the primary magma of the Yiyang komatiitic basalts are proposed to have MgO of 20% with a melting pressure up to 3 GPa (Wang et al., 2007), similar to the Gorgona komatiites, however, the primitive mantle–like Al_2O_3/TiO_2 ratios (21–23), enrichment in incompatible elements and unradiogenic Nd isotopes, suggest that their petrogenesis is different. In a previous study, Robin-Popieul et al. (2012) proposed a fresh perspective whereby the various types of komatiite represent liquids that escape from the source at different stages of the melting process. In their model, Al–depleted komatiites form first at about 13 GPa by equilibrium melting under conditions in which a large proportion of melt (30%–40%) was retained in the source and the residue contained abundant garnet (15%). Al–undepleted and Al–enriched komatiites from by fractional melting at intermediate to shallow depths after exhaustion of residual garnet. In this study, the Yiyang komatiitic basalts have primitive mantle–like Al_2O_3/TiO_2 ratios (21–23) and flat HREE patterns, similar to those of Al–undepleted or Munro–type komatiites (Sun and Nesbitt, 1978; Arndt et al., 2008). However, according to Robin-Popieul et al. (2012), the Al–undepleted or Munro–type komatiite commonly have depleted mantle (DM)–like lithophile isotopes and are strongly depleted in incompatible elements (Arndt et al., 2008), which was not observed in the Yiyang basalts. Instead, they show enrichment in LREE and other incompatible elements including LILE. This means that, unlike other Al–undepleted or Munro–type komatiites, the mantle source did not undergo earlier melting events, which would have consumed the enriched components of the mantle source (Robin-Popieul et al., 2012).

Additionally, recent studies on meimechite from the Siberian Traps Large Igneous Province (Ivanov et al., 2018), komatiites from the Abitibi greenstone belt in Canada (Sobolev et al., 2016), as well as basaltic rocks in many large intraplate igneous provinces, such as Karoo, Siberia, CAMP (Central Atlantic magmatic province), Columbia River, Emeishan, Deccan, and the Basin and Range Province (Wang et al., 2016), indicate that the primary melts of high-MgO members of LIPs are characterized by high H_2O concentrations. Several authors further proposed that the water may come from the mantle transition zone (e.g. Ivanov et al., 2018; Sobolev et al., 2016; Wang et al., 2016). Water–rich fluids will carry LILE such as Ba, Pb, K, and Sr, and LREE (La to Nd), but are not able to carry HFSEs such as Nb, Ta, and Ti (Wang et al., 2016). Therefore, the enrichment in LREE and LILE relative to the HSFE in the Yiyang komatiitic basalts can be explained by a deep volatile cycling model, with a possible relationship to stagnant oceanic slabs.

6. Conclusions

Based on our Os–Hf–Nd isotopic study of the ca. 825 Ma Yiyang basalts in the central SCB, we come to the following conclusions:

1) The Yiyang basalts have high Os contents (0.162–0.485 ppb; mostly > 0.3 ppb) and radiogenic Os compositions ($(^{187}Os/^{188}Os)_i$ = 0.134 to 0.282). Although AFC processes may have played a role in determining their whole–rock composition, the enrichment in LREE and LILE relative to the HSFE most likely reflect the nature of the primary magma.
2) The ca. 825 Ma Yiyang basalts and other contemporary high–MgO basalts in the central SCB have geochemical compositions distinct from typical boninites and are instead more closely aligned with komatiitic basalts. They were most likely generated within an intraplate setting.
3) Hafnium and Nd isotopes are decoupled in the Yiyang komatiitic basalts, suggesting that recycled sediments were incorporated into their source.

Supplementary data to this article can be found online at https://doi.org/10.1016/j.chemgeo.2018.10.027.

Acknowledgements

We are grateful to Dr. Laurie Reisberg, Dr. David van Acken and Editor Catherine Chauvel for their constructive comments. We thank C. M. Bao for assistance in field work and Z.Y. Chu, W.L. Ling, and J.F. Xu for assistance in Re−Os isotopic analyses. This work was supported by an Australian Research Council (ARC) Future Fellowship (FT140100826) and the National Natural Science Foundation of China (NNSFC; grant Nos.41373020 and 41702047).

References

van Acken, D., Becker, H., Walker, R.J., McDonough, W.F., Wombacher, F., Ash, R.D., Piccoli, P.M., 2010. Formation of pyroxenite layers in the Totalp ultramafic massif (Swiss Alps)–insights from highly siderophile elements and Os isotopes. Geochim. Cosmochim. Acta 74 (2), 661–683.
Ackerman, L., Bizimis, M., Haluzová, E., Sláma, J., Svojtka, M., Hirajima, T., Erban, V., 2016. Re–Os and Lu–Hf isotopic constraints on the formation and age of mantle pyroxenites from the Bohemian Massif. Lithos 256, 197–210.
Ackerman, L., Magna, T., Žák, K., Skála, R., Jonášová, Š., Mizera, J., Řanda, Z., 2017. The behavior of osmium and other siderophile elements during impacts: Insights from the Ries impact structure and central European tektites. Geochim. Cosmochim. Acta 210, 59–70.
Aitken, B.G., Echeverria, L.M., 1984. Petrology and geochemistry of komatiites and tholeiites from Gorgona-Island, Colombia. Contrib. Mineral. Petrol. 94–105.
Alves, S., Schiano, P., Allegre, C.J., 1999. Rhenium–osmium isotopic investigation of Java subduction zone lavas. Earth Planet. Sci. Lett. 168, 65–77.
Alves, S., Schiano, P., Capmas, F., Allegre, C.J., 2002. Osmium isotope binary mixing arrays in arc volcanism. Earth Planet. Sci. Lett. 198 (3–4), 355–369.
Arndt, N., 2003. Komatiites, kimberlites, and boninites. J. Geophys. Res. 108, B6.
Arndt, N.T., Jenner, G.A., 1986. Crustally contaminated komatiites and basalts from Kambalda, Western Australia. Chem. Geol. 56 (3–4), 229–255.
Arndt, N.T., Lesher, C.M., Barnes, S.J., 2008. Komatiite. Cambridge University Press, Cambridge, UK.
Beattie, 1994. Systematic and energetics of trace–element partitioning between olivine and silicate melts: Implications for the nature of mineral/melt partitioning. Chem. Geol. 117, 57–71.
Blichert-Toft, J., Frey, F.A., Albarède, F., 1999. Hf isotope evidence for pelagic sediments in the source of Hawaiian basalts. Science 285, 879–882.
Blichert-Toft, J., Arndt, N.T., Wilson, A., Coetzee, G., 2015. Hf and Nd isotope systematics of early Archean komatiites from surface sampling and ICDP drilling in the Barberton Greenstone Belt, South Africa. Am. Mineral. 100 (11 − 12), 2396–2411.
Borg, L.E., Brandon, A.D., Clynne, M.A., Walker, R.J., 2000. Re–Os isotopic systematics of primitive lavas from the Lassen region of the Cascade arc, California. Earth Planet. Sci. Lett. 177 (3–4), 301–317.
Brandon, A.D., Creaser, R.A., Shirey, S.B., Carlson, R.W., 1996. Osmium recycling in subduction zones. Science 272, 861–863.
Brandon, A.D., Walker, R.J., Puchtel, I.S., Becker, H., Humayun, M., Revillon, S., 2003. ^{186}Os–^{187}Os systematics of Gorgona Island komatiites: implications for early growth of the inner core. Earth Planet. Sci. Lett. 206 (3), 411–426.
Brenan, J.M., Bennett, N.R., Zajacz, Z., 2016. Experimental results on fractionation of the highly siderophile elements (HSE) at variable pressures and temperatures during planetary and magmatic differentiation. Rev. Mineral. Geochem. 81 (1), 1–87.
Burton, K.W., Gannoun, A., Birck, J.L., Allegre, C.J., Schiano, P., Clocchiatti, R., Alard, O., 2002. The compatibility of rhenium and osmium in natural olivine and their behavior during mantle melting and basalt genesis. Earth Planet. Sci. Lett. 198 (1–2), 63–76.
Cawood, P.A., Wang, Y.J., Xu, Y.J., Zhao, G.C., 2013. Locating South China in Rodinia and Gondwana: a fragment of greater India lithosphere? Geology 41, 903–906.
Chauvel, C., Lewin, E., Carpentier, M., Arndt, N.T., Marini, J.C., 2008. Role of recycled oceanic basalt and sediment in generating the Hf–Nd mantle array. Nat. Geosci. 1, 64–67.
Chauvel, C., Marini, J.C., Plank, T., Ludden, J.N., 2009. Hf–Nd input flux in the

Izu–Mariana subduction zone and recycling of subducted material in the mantle. Geochem. Geophys. Geosyst. 10 (1).
Che, Q.J., Peng, H.Q., Li, J.D., Jia, B.H., Wu, G.Y., Chen, B.H., 2005. Origin of the Yiyang paleovolcanic suite in northern Hunan, China, and its geological significance. Geol. Bull. China 24, 513–519 (in Chinese with English abstract).
Chen, K., Walker, R.J., Rudnick, R.L., Gao, S., Gaschnig, R.M., Puchtel, I.S., Tang, M., Hu, Z.C., 2016. Platinum–group element abundances and Re–Os isotopic systematics of the upper continental crust through time: evidence from glacial diamictites. Geochim. Cosmochim. Acta 191, 1–16.
Cohen, A.S., Waters, F.G., 1996. Separation of osmium from geological materials by solvent extraction for analysis by thermal ionisation mass spectrometry. Anal. Chim. Acta 332, 269–275.
Connolly, B.D., Puchtel, I.S., Walker, R.J., Arevalo, R., Piccoli, P.M., Byerly, G., Robin-Popieul, C., Arndt, N., 2011. Highly siderophile element systematics of the 3.3 Ga Weltevreden komatiites, South Africa: implications for early Earth history. Earth Planet. Sci. Lett. 311, 253–263.
Crawford, A.J., Falloon, T.J., Green, D.H., 1989. Classification, petrogenesis and tectonic setting of boninites. In: Boninites and Related Rocks, pp. 1–49.
Creaser, R.A., Papanastassiou, D.A., Wasserburg, G.J., 1991. Negative thermal ion mass spectrometry of osmium, rhenium and iridium. Geochim. Cosmochim. Acta 55, 397–401.
Day, J.M.D., 2013. Hotspot volcanism and highly siderophile elements. Chem. Geol. 341, 50–74.
DePaolo, D.J., 1981. Trace element and isotopic effects of combined wallrock assimilation and fractional crystallization. Earth Planet. Sci. Lett. 53 (2), 189–202.
Dong, S.W., Gao, R., Yin, A., Guo, T.L., Zhang, Y.Q., Hu, J.M., Li, J.H., Shi, W., Li, Q.S., 2013. What drove continued continent–continent convergence after ocean closure? Insights from high-resolution seismic reflection profiling across the Daba Shan in central China. Geology 41 (6), 671–674.
Dong, S.W., Zhang, Y.Q., Gao, R., Su, J.B., Liu, M., Li, J.H., 2015. A possible buried Paleoproterozoic collisional orogen beneath central South China: evidence from seismic–reflection profiling. Precambrian Res. 264, 1–10.
Escrig, S., Schiano, P., Schilling, J.G., Allegre, C., 2005. Rhenium–osmium isotope systematics in MORB from the Southern Mid–Atlantic Ridge (408°–508° S). Earth Planet. Sci. Lett. 235, 528–548.
Fan, J., Kerrich, R., 1997. Geochemical characteristics of aluminum depleted and undepleted komatiites and HREE-enriched low-Ti tholeiites, western Abitibi greenstone belt: a heterogeneous mantle plume-convergent margin environment. Geochim. Cosmochim. Acta 61 (22), 4723–4744.
Gannoun, A., Burton, K.W., Barfod, D.N., Schiano, P., Vlastélic, I., Halliday, A.N., 2015. Resolving mantle and magmatic processes in basalts from the Cameroon volcanic line using the Re–Os isotope system. Lithos 224, 1–12.
Gannoun, A., Burton, K.W., Day, J.M.D., Harvey, J., Schiano, P., Parkinson, I., 2016. Highly siderophile element and Os isotope systematics of volcanic rocks at divergent and convergent plate boundaries and in intraplate settings. Rev. Mineral. Geochem. 81, 651–724.
Golowin, R., Portnyagin, M., Hoernle, K., Hauff, F., Gurenko, A., Garbe-Schonberg, D., Werner, R., Turner, S., 2017. Boninite-like intraplate magmas from Manihiki Plateau require ultra-depleted and enriched source components. Nat. Commun. 8. https://doi.org/10.1038/ncomms14322.
Grove, T.L., Parman, S.W., 2004. Thermal evolution of the Earth as recorded by komatiites. Earth Planet. Sci. Lett. 219, 173–187.
Guo, L.Q., Tang, X.S., Pen, H.Q., 2003. The Sm–Nd isotopic ages of the early Precambrian mafic-ultramafic volcanic rocks in Yiyang, Hunan. Geol. Miner. Resour. South China 2, 46–51 (in Chinese, with English abstract).
Harvey, J., Gannoun, A., Burton, K.W., Rogers, N.W., Alard, O., Parkinson, I.J., 2006. Ancient melt extraction from the oceanic upper mantle revealed by Re–Os isotopes in abyssal peridotites from the Mid–Atlantic ridge. Earth Planet. Sci. Lett. 244 (3), 606–621.
Herzberg, C., 1995. Generation of plume magmas through time–an experimental perspective. Chem. Geol. 126 (1), 1–16.
Herzberg, C., Asimow, P.D., 2008. Petrology of some oceanic island basalts: PRIMELT2.XLS software for primary magma calculation. Geochem. Geophys. Geosyst. 9 (9).
Herzberg, C., Asimow, P.D., Arndt, N., Niu, Y., Lesher, C.M., Fitton, J.G., Saunders, A.D., 2007. Temperature in ambient mantle and plumes: Constraints from basalts, picrites, and komatiites. Geochem. Geophys. Geosyst. 8 (2).
Hollings, P., Wyman, D., Kerrich, R., 1999. Komatiite-basalt-rhyolite volcanic associations in northern Superior Province greenstone belts; significance of plume-arc interaction in the generation of the proto continental Superior Province. Lithos 46, 137–161.
Huppert, H.E., Stephen, R., Sparks, J., 1985. Cooling and contamination of mafic and ultra–mafic magmas during ascent through continental crust. Earth Planet. Sci. Lett. 74 (4), 371–386.
Ivanov, A.V., Mukasa, S.B., Kamenetsky, V.S., Ackerson, M., Demonterova, E.I., Pokrovsky, B.G., Vladykin, N.V., Kolesnichenko, M.V., Litasov, K.D., Zedgenizov, D.A., 2018. Volatile concentrations in olivine–hosted melt inclusions from meimechite and melanephelinite lavas of the Siberian Traps Large Igneous Province: evidence for flux–related high–Ti, high–Mg magmatism. Chem. Geol. 483, 442–462.
Kerr, A.C., 2005. La Isla de Gorgona, Colombia: a petrological enigma? Lithos 84 (1–2), 77–101.
Kleinhanns, I.C., Kreissig, K., Kamber, B.S., Meisel, T., Nagler, T.F., Kramers, J.D., 2002. Combined chemical separation of Lu, Hf, Sm, Nd, and REEs from a single rock digest: Precise and accurate isotope determinations of Lu-Hf and Sm-Nd using multi-collector-ICPMS. Anal. Chem. 74, 67–73.
Konig, S., Munker, C., Schuth, S., Luguet, A., Hoffmann, J.E., Kuduon, J., 2010. Boninites as windows into trace element mobility in subduction zones. Geochim. Cosmochim. Acta 74, 684–704.
Langmuir, C.H., Klein, E.M., Plank, T., 1992. Petrological systematics of mid-ocean ridge basalts: Constraints on melt generation beneath ocean ridges. In: Morgan, J.P. (Ed.), Mantle Flow and Melt Generation at Mid-ocean Ridges. vol. 71. Am. Geophys. Union Geophys. Monogr., pp. 183–280.
Le Bas, M.J., 2000. IUGS reclassification of the high-Mg and picritic volcanic rocks. J. Petrol. 41, 1467–1470.
Lee, C.T.A., Luffi, P., Chin, E.J., Bouchet, R., Dasgupta, R., Morton, D.M., Le Roux, V., Yin, Q.Z., Jin, D., 2012. Copper systematics in arc magmas and implications for crust-mantle differentiation. Science 336, 64–68.
Li, Z.X., Zhang, L.H., McApowell, C., 1995. South China in Rodinia: part of the missing link between Australia–East Antarctica and Laurentia? Geology 23, 407–410.
Li, Z.X., Li, X.H., Kinny, P.D., Wang, J., Zhang, S., Zhou, H., 2003a. Geochronology of Neoproterozoic syn–rift magmatism in the Yangtze Craton, South China and correlations with other continents: evidence for a mantle superplume that broke up Rodinia. Precambrian Res. 122, 85–109.
Li, X.H., Li, Z.X., Ge, W.C., Zhou, H.W., Li, W.X., Liu, Y., Wingate, M.T.D., 2003b. Neoproterozoic granitoids in South China: crustal melting above a mantle plume at ca. 825 Ma? Precambrian Res. 122, 45–83.
Li, X.H., Liu, D.Y., Sun, M., Li, W.X., Liang, X.R., Liu, Y., 2004. Precise Sm–Nd and U–Pb isotopic dating of the super–giant Shizhuyuan polymetallic deposit and its host granite, Southeast China. Geol. Mag. 141, 225–231.
Li, Z.X., Wartho, J.A., Occhipinti, S., Zhang, C.L., Li, X.H., Wang, J., Bao, C.M., 2007a. Early history of the eastern Sibao Orogen (South China) during the assembly of Rodinia: new mica $^{40}Ar/^{39}Ar$ dating and SHRIMP U–Pb detrital zircon provenance constraints. Precambrian Res. 159, 79–94.
Li, X.H., Liu, Y., Yang, Y.H., Chen, F.K., Tu, X.L., Qi, C.S., 2007b. Rapid separation of Lu–Hf and Sm–Nd from a single rock dissolution and precise measurement of Hf–Nd isotopic ratios for national rock standards. Acta Petrol. Sin. 23, 221–226.
Li, J., Liang, X.R., Dong, Y.H., Tu, X.L., Xu, J.F., 2007c. Measurements of Re-Os isotopic compositions in mafic–ultramafic rocks by multi–collector inductively coupled plasma mass spectrometer (MC–ICPMS). Geochimica 36, 153–160 (In Chinese with English abstract).
Li, Z.X., Bogdanova, S.V., Collins, A.S., Davidson, A., De Waele, B., Ernst, R.E., Fitzsimons, I.C.W., Fuck, R.A., Gladkochub, D.P., Jacobs, J., Karlstrom, K.E., Lu, S., Natapov, L.M., Pease, V., Pisarevsky, S.A., Thrane, K., Vernikovsky, V., 2008. Assembly, configuration, and break–up history of Rodinia: a synthesis. Precambrian Res. 160, 179–210.
Li, X.H., Li, W.X., Li, Z.X., Lo, C.H., Wang, J., Ye, M.F., Yang, Y.H., 2009. Amalgamation between the Yangtze and Cathaysia Blocks in South China: constraints from SHRIMP U–Pb zircon ages, geochemistry and Nd–Hf isotopes of the Shuangxiwu volcanic rocks. Precambrian Res. 174, 117–128.
Li, X.H., Li, W.X., Li, Z.X., Lo, C.H., Wang, J., Ye, M.F., Yang, Y.H., 2010a. Petrogenesis and tectonic significance of the ~850 Ma Gangbian alkaline complex in South China: evidence from in situ zircon U–Pb dating, Hf–O isotopes and whole–rock geochemistry. Lithos 114, 1–15.
Li, W.X., Li, X.H., Li, Z.X., 2010b. Ca. 850 Ma bimodal volcanic rocks in northeastern Jiangxi Province, South China: initial extension during the breakup of Rodinia? Am. J. Sci. 310, 951–980.
Li, J., Zhao, P.P., Liu, J.G., Wang, X.C., Yang, Y., Wang, G.Q., Xu, J.F., 2015a. Reassessment of hydrofluoric acid desilicification in the Carius tube digestion technique for Re-Os isotopic analysis in geological samples. Geostand. Geoanal. Res. 39, 17–30.
Li, J., Wang, X.C., Xu, J.F., Xu, Y.G., Tang, G.J., Wang, Q., 2015b. Disequilibrium-induced initial Os isotopic heterogeneity in gramaliquots of single basaltic rock powders: Implications for dating and source tracing. Chem. Geol. 406, 10–17.
Lissner, M., König, S., Luguet, A., le Roux, P.J., Schuth, S., Heuser, A., le Roex, A.P., 2014. Selenium and tellurium systematics in MORBs from the southern Mid–Atlantic Ridge (47–50 S). Geochim. Cosmochim. Acta 144, 379–402.
Liu, C.Z., Snow, J.E., Hellebrand, E., Brugmann, G., von der Handt, A., Buchl, A., Hofmann, A.W., 2008. Ancient, highly heterogeneous mantle beneath Gakkel ridge, Arctic Ocean. Nature 452, 311–316.
Luttinen, A.V., Rämö, O.T., Huhma, H., 1998. Neodymium and strontium isotopic and trace element composition of a Mesozoic CFB suite from Dronning Maud Land, Antarctica: implications for lithosphere and asthenosphere contributions to Karoo magmatism. Geochim. Cosmochim. Acta 62 (15), 2701–2714.
Lyu, P.L., Li, W.X., Wang, X.C., Pang, C.J., Cheng, J.X., Li, X.H., 2017. Initial breakup of supercontinent Rodinia as recorded by ca 860–840 Ma bimodal volcanism along the southeastern margin of the Yangtze Block, South China. Precambrian Res. 296, 148–167.
McKenzie, D., Bickle, M.J., 1988. The volume and composition of melt generated by extension of the lithosphere. J. Petrol. 29, 625–679.
Meisel, T., Walker, R.J., Irving, A.J., Lorand, J.P., 2001. Osmium isotopic compositions of mantle xenoliths: a global perspective. Geochim. Cosmochim. Acta 65, 1311–1323.
Nier, A.O., 1973. The isotopic constitution of osmium. Phys. Rev. 52, 885–892.
Parman, S.W., Grove, T.L., Dann, J.C., de Wit, M.J., 2004. A subduction origin for komatiites and cratonic lithospheric mantle. S. Afr. J. Geol. 107, 107–118.
Patchett, P.J., White, W.M., Feldmann, H., Kielinczuk, S., Hofmann, A.W., 1984. Hafnium/rare earth element fractionation in the sedimentary system and crustal recycling into the Earth's mantle. Earth Planet. Sci. Lett. 69, 365–378.
Pearce, J.A., Norry, M.J., 1979. Petrogenetic implications of Ti, Zr, Y, and Nb variations in volcanic rocks. Contrib. Mineral. Petrol. 69 (1), 33–47.
Pearson, D.G., Nowell, G.M., 2004. Re–Os and Lu–Hf isotope constraints on the origin and age of pyroxenites from the Beni Bousera peridotite massif: implications for mixed peridotite–pyroxenite mantle sources. J. Petrol. 45 (2), 439–455.

Pearson, D.G., Woodland, S.J., 2000. Solvent extraction/anion exchange separation and determination of PGEs (Os, Ir, Pt, Pd, Ru) and Re–Os isotopes in geological samples by isotope dilution ICP–MS. Chem. Geol. 165, 87–107.
Puchtel, I.S., Haase, K.M., Hofmann, A.W., Chauvel, C., Kulikov, V.S., Garbe-Schönberg, C.D., Nemchin, A.A., 1997. Petrology and geochemistry of crustally contaminated komatiitic basalts from the Vetreny Belt, southeastern Baltic shield: evidence for an early Proterozoic mantle plume beneath rifted Archean continental lithosphere. Geochim. Cosmochim. Acta 61, 1205–1222.
Puchtel, I.S., Brandon, A.D., Humayun, M., 2004. Precise Pt–Re–Os isotope systematics of the mantle from 2.7-Ga komatiites. Earth Planet. Sci. Lett. 224, 157–174.
Puchtel, I.S., Brandon, A.D., Humayun, M., Walker, R.J., 2005. Evidence for the early differentiation of the core from Pt–Re–Os isotope systematics of 2.8-Ga komatiites. Earth Planet. Sci. Lett. 237, 118–134.
Puchtel, I.S., Walker, R.J., Brandon, A.D., Nisbet, E.G., 2009. Pt–Re–Os and Sm–Nd isotope and HSE and REE systematics of the 2.7 Ga Belingwe and Abitibi komatiites. Geochim. Cosmochim. Acta 73, 6367–6389.
Puchtel, I.S., Walker, R.J., Touboul, M., Nisbet, E.G., Byerly, G.R., 2014. Insights into early Earth from the Pt–Re–Os isotope and highly siderophile element abundance systematics of Barberton komatiites. Geochim. Cosmochim. Acta 125, 394–413.
Putirka, K.D., 2005. Mantle potential temperatures at Hawaii, Iceland, and the mid-ocean ridge system, as inferred from olivine phenocrysts: evidence for thermally driven mantle plume. Geochem. Geophys. Geosyst. 6 (5).
Reagan, M.K., Ishizuka, O., Stern, R.J., Kelley, K.A., Ohara, Y., Blichert-Toft, J., Bloomer, S.H., Cash, J., Fryer, P., Hanan, B.B., Hickey-Vargas, R., Ishii, T., Kimura, J.I., Peate, D.W., Rowe, M.C., Wood, M., 2010. Fore–arc basalts and subduction initiation in the Izu–Bonin–Mariana system. Geochem. Geophys. Geosyst. 11 (3).
Righter, K., Chesley, J.T., Calazza, C.M., Gibson, E.K., Ruiz, J., 2008. Re and Os concentrations in arc basalts: the roles of volatility and source region fO2 variations. Geochim. Cosmochim. Acta 72, 926–947.
Robin-Popieul, C.C., Arndt, N.T., Chauvel, C., Byerly, G.R., Sobolev, A.V., Wilson, A., 2012. A new model for Barberton komatiites: deep critical melting with high melt retention. J. Petrol. 53 (11), 2191–2229.
Roy-Barman, M., Luck, J.M., Allégre, C.J., 1996. Os isotopes in orogenic lherzolite massifs and mantle heterogeneities. Chem. Geol. 130, 55–64.
Rudnick, R.L., Gao, S., 2003. Composition of the continental crust. In: Treatise on Geochemistry. 3. pp. 659.
Saal, A.E., Rudnick, R.L., Ravizza, G.E., Hart, S.R., 1998. Re–Os isotope evidence for the composition, formation and age of the lower continental crust. Nature 393 (6680), 58.
Senda, R., Shimizu, K., Suzuki, K., 2016. Ancient depleted mantle as a source of boninites in the Izu–Bonin–Mariana arc: evidence from Os isotopes in Cr–spinel and magnetite. Chem. Geol. 439, 100–119.
Shervais, J.W., 1982. Ti–V plots and the petrogenesis of modern and ophiolitic lavas. Earth Planet. Sci. Lett. 59 (1), 101–118.
Shirey, S.B., Walker, R.J., 1995. Carius tube digestion for low blank rhenium–osmium analyses. Anal. Chem. 34, 2136–2141.
Shirey, S.B., Walker, R.J., 1998. The Re–Os isotope system in cosmochemistry and high–temperature geochemistry. Annu. Rev. Earth Planet. Sci. 26, 423–500.
Shirey, S.B., Berg, J.H., Carlson, R.W., 1994. Temporal changes in the sources of flood basalts: isotopic and trace element evidence from the 1100 Ma old Keweenawan Mamainse Point Formation, Ontario, Canada. Geochim. Cosmochim. Acta 58 (20), 4475–4490.
Sobolev, A.V., Danyushevsky, L.V., 1994. Petrology and geochemistry of Boninites from the North Termination of the Tonga Trench–constraints on the generation conditions of primary high–Ca Boninite magmas. J. Petrol. 35, 1183–1211.
Sobolev, A.V., Hofmann, A.W., Kuzmin, D.V., Yaxley, G.M., Arndt, N.T., Chung, S.L., Danyushevsky, L.V., Elliott, T., Frey, F.A., Garcia, M.O., Gurenko, A.A., Kamenetsky, V.S., Kerr, A.C., Krivolutskaya, N.A., Matvienkov, V.V., Nikogosian, I.K., Rocholl, A., Sigurdsson, I.A., Sushchevskaya, T.M., Teklay, M., 2007. The amount of recycled crust in sources of mantle-derived melts. Science 316 (5823), 412–417.
Sobolev, A.V., Asafov, A.V., Gurenko, A.A., Arndt, N.T., Batanova, V.G., Portnyagin, M.V., Garbe-Schönberg, D., Krasheninnikov, S.P., 2016. Komatiites reveal a hydrous Archaean deep–mantle reservoir. Nature 531 (7596), 628–632.
Stracke, A., Bizimis, M., Salters, V.J.M., 2003. Recycling oceanic crust: Quantitative constraints. Geochem. Geophys. Geosyst. 4, 8003.
Sun, S.S., McDonough, W.F., 1989. Chemical and isotopic systematics of oceanic basalts: implications for mantle composition and processes. In: Saunders, A.D., Norry, M.J. (Eds.), Magmatism in the Ocean Basins. vol. 41. Geol. Soc. London, Spec. Publ., pp. 313–345.
Sun, S.S., Nesbitt, R.W., 1978. Petrogenesis of Archaean ultrabasic and basic volcanics: evidence from rare earth elements. Contrib. Mineral. Petrol. 65 (3), 301–325.
Suzuki, K., Senda, R., Shimizu, K., 2011. Osmium behavior in a subduction system elucidated from chromian-spinel in Bonin Island beach sands. Geology 39, 999–1002.
Tanaka, T., Togashi, S., Kamioka, H., Amakawa, H., Kagami, H., Hamamoto, T., Yuhara, M., Orihashi, Y., Yoneda, S., Shimizu, H., Kunimaru, T., Takahashi, K., Yanagi, T., Nakano, T., Fujimaki, H., Shinjo, R., Asahara, Y., Tanimizu, M., Dragusanu, C., 2000. JNdi-1: a neodymium isotopic reference in consistency with La Jolla neodymium. Chem. Geol. 168, 279–281.
Taylor, R.N., Nesbitt, R.W., Vidal, P., Harmon, R.S., Auvray, B., Croudace, I.W., 1994. Mineralogy, chemistry and genesis of the boninite series volcanics, Chichijima, Bonin Islands, Japan. J. Petrol. 35, 577–617.
Todd, E., Gill, J.B., Pearce, J.A., 2012. A variably enriched mantle wedge and contrasting melt types during arc stages following subduction initiation in Fiji and Tonga, southwest Pacific. Earth Planet. Sci. Lett. 335, 180–194.
Turner, S., Handler, M., Bindeman, I., Suzuki, K., 2009. New insights into the origin of O–Hf–Os isotope signatures in arc lavas from Tonga–Kermadec. Chem. Geol. 266 (3–4), 187–193.
Van Acken, D., Hoffmann, J.E., Schorscher, J.H.D., Schulz, T., Heuser, A., Luguet, A., 2016. Formation of high–Al komatiites from the Mesoarchean Quebra Osso Group, Minas Gerais, Brazil: trace elements, HSE systematics and Os isotopic signatures. Chem. Geol. 422, 108–121.
Vervoort, J.D., Patchett, P.J., Blichert-Toft, J., Albarede, F., 1999. Relationships between Lu–Hf and Sm–Nd isotopic systems in the global sedimentary system. Earth Planet. Sci. Lett. 168, 79–99.
Vervoort, J.D., Plank, T., Prytulak, J., 2011. The Hf–Nd isotopic composition of marine sediments. Geochim. Cosmochim. Acta 75, 5903–5926.
Volkening, J., Walczyk, T., Heumannm K., G., 1991. Osmium isotope ratio determinations by negative thermal ionization mass spectrometry. Int. J. Mass Spectrom. Ion Process. 105, 147–159.
Wang, J., Li, Z.X., 2003. History of Neoproterozoic rift basins in South China: implications for Rodinia break–up. Precambrian Res. 122, 141–158.
Wang, J., Li, X.H., Duan, T.Z., Liu, D.Y., Song, B., Li, Z.X., Gao, Y.H., 2003. New evidences on zircon SHRIMP U-Pb dating for the Cangshuipu volcanic rocks and its implications for the basal boundary of the “Nanhuan” strata in South China. Chin. Sci. Bull. 48, 1663–1669.
Wang, X.C., Li, X.H., Li, W.X., Li, Z.X., 2007. Ca. 825 Ma komatiitic basalts in South China: first evidence for > 1500 °C mantle melts by a Rodinian mantle plume. Geology 35 (12), 1103–1106.
Wang, X.C., Li, X.H., Li, W.X., Li, Z.X., Liu, Y., Yang, Y.H., Liang, X.R., Tu, X.L., 2008. The Bikou basalts in the northwestern Yangtze block, South China: Remnants of 820–810 Ma continental flood basalts? Geol. Soc. Am. Bull. 120 (11), 1478–1492.
Wang, X.C., Li, X.H., Li, W.X., Li, Z.X., 2009. Variable involvements of mantle plumes in the genesis of mid–Neoproterozoic basaltic rocks in South China: a review. Gondwana Res. 15 (3–4), 381–395.
Wang, X.C., Li, Z.X., Li, X.H., Li, Q.L., Tang, G.Q., Zhang, Q.R., Liu, Y., 2011. Nonglacial origin for low–^{18}O Neoproterozoic magmas in the South China Block: evidence from new in–situ oxygen isotope analyses using SIMS. Geology 39, 735–738.
Wang, X.C., Wilde, S.A., Xu, B., Pang, C.J., 2016. Origin of arc–like continental basalts: implications for deep–Earth fluid cycling and tectonic discrimination. Lithos 261, 5–45.
Widom, E., 2011. Recognizing recycled osmium. Geology 39 (11), 1087–1088.
Widom, E., Kepezhinskas, P., Defant, M., 2003. The nature of metasomatism in the sub-arc mantle wedge: evidence from Re–Os isotopes in Kamchatka peridotite xenoliths. Chem. Geol. 196, 283–306.
Wilson, A.H, 2003. A new class of silica enriched, highly depleted komatiites in the southern Kaapvaal Craton, South Africa. Precambrian Res. 127 (1), 125–141.
Woodhead, J., Brauns, M., 2004. Current limitations to the understanding of Re–Os behaviour in subduction systems, with an example from New Britain: Earth Planet. Sci. Lett. 221, 309–323.
Wu, T., Zhou, J.X., Wang, X.C., Li, W.X., Wilde, S.A., Sun, H.R., Wang, J.S., Li, Z., 2018. Identification of ca. 850 Ma high-temperature strongly peraluminous granitoids in southeastern Guizhou Province, South China: a result of early extension along the southern margin of the Yangtze Block. Precambrian Res. 308, 18–34.
Xiao, X.D., 1988. Spinifex was found in Mesoproterozoic Komatiites of Yiyang, Hunan. Chin. Sci. Bull. 4, 286–288 (in Chinese).
Xiao, L., Xu, Y.G., Mei, H.J., Zheng, Y.F., He, B., Pirajno, F., 2004. Distinct mantle sources of low-Ti and high-Ti basalts from the western Emeishan large igneous province, SW China: implications for plume–lithosphere interaction. Earth Planet. Sci. Lett. 228 (3), 525–546.
Yang, C., Li, X.H., Wang, X.C., Lan, Z.W., 2015. Mid–Neoproterozoic angular unconformity in the Yangtze Block revisited: insights from detrital zircon U–Pb age and Hf–O isotopes. Precambrian Res. 266, 165–178.
Zhang, Y.Z., Wang, Y.J., Zhang, Y.H., Zhang, A.M., 2015. Neoproterozoic assembly of the Yangtze and Cathaysia blocks: evidence from the Cangshuipu Group and associated rocks along the Central Jiangnan Orogen, South China. Precambrian Res. 269, 18–30.
Zhang, J., Li, J., Long, X.P., Sun, S.L., Yin, L., Dai, M.N., 2017. Rhenium–osmium isotope measurements of geological reference material BIR–1a: evaluation of homogeneity and implications for method validation and quality control. Geostand. Geoanal. Res. https://doi.org/10.1111/ggr.12180.
Zhao, J.H., Asimow, P.D., 2014. Neoproterozoic boninite-series rocks in South China: a depleted mantle source modified by sediment-derived melt. Chem. Geol. 388, 98–111.
Zhao, G.C., Cawood, P.A., 1999. Tectonothermal evolution of the Mayuan assemblage in the Cathaysia Block: implications for Neoproterozoic collision–related assembly of the South China Craton. Am. J. Sci. 299, 309–339.
Zhao, G.C., Cawood, P.A., 2012. Precambrian geology of China. Precambrian Res. 222–223, 13–54.
Zhao, J.H., Zhou, M.F., 2013. Neoproterozoic high–Mg basalts formed by melting of ambient mantle in South China. Precambrian Res. 233, 193–205.
Zhao, J.H., Zhou, M.F., Yan, D.P., Zheng, J.P., Li, J.W., 2011. Reappraisal of the ages of Neoproterozoic strata in South China: no connection with the Grenvillian orogeny. Geology 39, 299–302.
Zhou, M.F., Yan, D.P., Kennedy, A.K., Li, Y., Ding, J., 2002. SHRIMP U–Pb zircon geochronological and geochemical evidence for Neoproterozoic arc-magmatism along the western margin of the Yangtze Block, South China. Earth Planet. Sci. Lett. 196, 51–67.
Zhou, M.F., Ma, Y.X., Yan, D.P., Xia, X.P., Zhao, J.H., Sun, M., 2006. The Yanbian Terrane (Southern Sichuan Province, SW China): a Neoproterozoic arc assemblage in the western margin of the Yangtze Block. Precambrian Res. 144, 19–38.